haematologica
Journal of the Ferrata Storti Foundation

BTK/BCL2 dual targeting enhances apoptosis in marginal zone lymphoma: preclinical activity of tacabrutideg (BGB-16673) and sonrotoclax

by Alberto J. Arribas, Alex Zadro, Elisa Civanelli, Giulio Sartori, Camilla Scalise, Luciano Cascione, Riccardo Moia, Nawar Maher, Laura Carosella, Stefano Raniolo, Andrea Rinaldi, Chiara Arrigoni, Davide Rossi, Emanuele Zucca, Gianluca Gaidano, Matteo Moretti, Vittorio Limongelli and Francesco Bertoni

Received: February 24, 2026.
Accepted: September 22, 2026.

Citation: Alberto J. Arribas, Alex Zadro, Elisa Civanelli, Giulio Sartori, Camilla Scalise, Luciano Cascione, Riccardo Moia, Nawar Maher, Laura Carosella, Stefano Raniolo, Andrea Rinaldi, Chiara Arrigoni, Davide Rossi, Emanuele Zucca, Gianluca Gaidano, Matteo Moretti, Vittorio Limongelli and Francesco Bertoni. BTK/BCL2 dual targeting enhances apoptosis in marginal zone lymphoma: preclinical activity of tacabrutideg (BGB-16673) and sonrotoclax.
Haematologica. 2026 Oct 1. doi: 10.3324/haematol.2026.300780 [Epub ahead of print]

Publisher's Disclaimer.
E-publishing ahead of print is increasingly important for the rapid dissemination of science. Haematologica is, therefore, E-publishing PDF files of an early version of manuscripts that have completed a regular peer review and have been accepted for publication.
E-publishing of this PDF file has been approved by the authors.
After having E-published Ahead of Print, manuscripts will then undergo technical and English editing, typesetting, proof correction and be presented for the authors' final approval, the final version of the manuscript will then appear in a regular issue of the journal.
All legal disclaimers that apply to the journal also pertain to this production process.

BTK/BCL2 dual targeting enhances apoptosis in marginal zone lymphoma: preclinical activity of tacabrutideg (BGB-16673) and sonrotoclax

Alberto J. Arribas [1,2], Alex Zadro [1,3], Elisa Civanelli [1], Giulio Sartori [1], Camilla Scalise [1], Luciano Cascione [1,2], Riccardo Moia [4], Nawar Maher [4], Laura Carosella [5], Stefano Raniolo [5], Andrea Rinaldi [1], Chiara Arrigoni [3], Davide Rossi [1,6], Emanuele Zucca [1,6], Gianluca Gaidano [4], Matteo Moretti [3], Vittorio Limongelli [5], Francesco Bertoni [1,6].

[1] Institute of Oncology Research, Faculty of Biomedical Sciences, USI, Bellinzona, Switzerland;
[2] SIB Swiss Institute of Bioinformatics, Lausanne, Switzerland;
[3] Regenerative Medicine Division, Institute for Translational Research, Faculty of Biomedical Sciences, Università Della Svizzera Italiana (USI)-Ente Ospedaliero Cantonale (EOC), Bellinzona, Switzerland;
[4] Division of Hematology, Department of Translational Medicine, University of Eastern Piedmont, Novara, Italy;
[5] Euler Institute, Faculty of Biomedical Sciences, Università della Svizzera italiana (USI), Lugano, Switzerland.
[6] Oncology Institute of Southern Switzerland, Ente Ospedaliero Cantonale, Bellinzona, Switzerland

Corresponding authors:

- Prof. Francesco Bertoni, Institute of Oncology Research, via Francesco Chiesa 5, 6500 Bellinzona, Switzerland. Phone: +41 58 666 7206; e-mail: francesco.bertoni@ior.usi.ch
- Dr. Alberto J. Arribas, Institute of Oncology Research, via Francesco Chiesa 5, 6500 Bellinzona, Switzerland. Phone: +41 58 666 7202; e-mail: alberto.arribas@ior.usi.ch

Conflicts of interests

Alberto J. Arribas: travel grant from Astra Zeneca and Floratek Pharma, advisory board fee from PentixaPharm. Luciano Cascione: institutional research funds from Orion; travel grant from HTG. Emanuele Zucca: institutional research funds from Celgene, Roche and Janssen; advisory board fees from Celgene, Roche, Mei Pharma, Astra Zeneca and Celltrion Healthcare; travel grants from Abbvie and Gilead; expert statements provided to Gilead, Bristol-Myers Squibb and MSD. Davide Rossi: grant support from Gilead, AbbVie, Janssen; honoraria from Gilead, AbbVie Janssen, Roche; scientific advisory board fees from Gilead, AbbVie, Janssen, AstraZeneca, MSD. Francesco Bertoni: institutional research funds from ADC Therapeutics, Bayer AG, BeiGene, Floratek Pharma, Helsinn, HTG Molecular Diagnostics, Ideogen AG, Idorsia Pharmaceuticals Ltd., Immagene, ImmunoGen, Menarini Ricerche, Nordic Nanovector ASA, Oncternal Therapeutics, Spexis AG; consultancy fee from BIMINI Biotech, Floratek Pharma, Helsinn, Immagene, Menarini, Vrise Therapeutics; advisory board fees to institution from Novartis; expert statements provided to HTG Molecular Diagnostics; travel grants from Amgen, Astra Zeneca, iOnctura.
The other Authors have nothing to disclose.

Authors' contributions

AJA performed experiments, analyzed and interpreted data, performed data mining, prepared the figures, and co-wrote the manuscript.
L Cascione performed data mining.
AZ, EC, CS, GS: performed experiments.
L Carosella SR, VL: performed modeling computational studies.
RM, NM: provided MZL primary cells.
CA, EZ, GG, MM, DR: provided advice.
AR performed transcriptome profiling.
FB co-designed research, interpreted data, and co-wrote the manuscript.
All authors reviewed and accepted the final version of the manuscript.

Acknowledgements

Not applicable.

Availability of data and materials

The datasets generated and/or analysed during the current study are available in the [National Center for Biotechnology Information (NCBI) Gene Expression Omnibus (GEO; http://www.ncbi.nlm.nih.gov/geo) database (GSE312595).

Funding

This work was partially supported by institutional research funds from Beigene, the Swiss National Science Foundation (SNSF 31003A_163232/1) (DR, EZ, FB), Swiss Cancer Research (KFS-4727-02-2019) (FB), the European Research Council (ERC) under the European Union's Horizon 2020 research and innovation programme ("CoMMBi" ERC grant agreement No.101001784) (VL), and a grant from the Swiss National Supercomputing Centre (CSCS) under project ID u8 (VL). Fond'Action contre le Cancer (AZ).

Abstract
Bruton tyrosine kinase (BTK) and BCL2 are key therapeutic targets in marginal zone lymphoma (MZL). We evaluated the novel BTK degrader tacabrutideg (BGB-16673) and the second-generation BCL2 inhibitor sonrotoclax, alone and in combination, in MZL models, including derivatives with acquired resistance to BTK, BCL2, and PI3K inhibitors. Tacabrutideg was evaluated for cytotoxicity, apoptosis, transcriptomic and protein changes, real-time cell growth, three-dimensional stromal co-culture, and activity in primary MZL samples. Combination studies included sonrotoclax, venetoclax, bendamustine, lenalidomide, rituximab, selinexor, and tazemetostat.Tacabrutideg showed single-agent activity in MZL cell lines, inducing BTK degradation and suppression of BCR signaling, MYC targets, and oxidative phosphorylation. Its biological effects largely overlapped with those of zanubrutinib while maintaining complete target degradation. Tacabrutideg inhibited PLCG2 and ERK phosphorylation, reduced cell growth in real-time assays, retained activity in three-dimensional stromal co-cultures, and suppressed growth and ERK phosphorylation in primary MZL samples. Combination studies identified the greatest benefit with sonrotoclax, venetoclax, bendamustine, lenalidomide, and rituximab. Sonrotoclax consistently outperformed venetoclax, exhibiting >10-fold greater potency in three MZL cell lines and synergizing with tacabrutideg across multiple models. The combination enhanced apoptosis through coordinated modulation of BCL2 family proteins, including BCL2, MCL1, and BCL-XL. Tacabrutideg demonstrates potent preclinical activity in MZL as a single agent and in combination regimens. Together with the superior activity of sonrotoclax, these findings provide a strong rationale for the clinical evaluation of dual BTK degradation and BCL2 inhibition in patients with MZL.

Introduction

B cell receptor (BCR) signaling and the apoptotic machinery are crucial pathways for the proliferation and survival of B cells. Their pharmacological inhibition with small molecules targeting BTK and BCL2 has proven their clinical efficacy for treating patients affected by lymphoid neoplasms, including marginal zone lymphoma (MZL)(1-5).

Depending on the country, six BTK inhibitors (ibrutinib, zanubrutinib, acalabrutinib, orelabrutinib, tirabrutinib, and pirtobrutinib) and the first-generation BCL2 inhibitor venetoclax are approved for the treatment of patients with various mature B-cell lymphoid tumors. Notably, data from clinical trials led to approval of ibrutinib (6), zanubrutinib (7), and orelabrutinib (8) specifically for MZL patients. Conversely, clinical data with the first-in-class BCL2 inhibitor venetoclax as a single agent are limited to the patients (overall response (ORR) rate 67%) enrolled in the initial phase 2 study evaluating the drug in the refractory/relapsed (R/R) setting (5), albeit additional preclinical and clinical data are available in combination with other drugs (9, 10).

Unfortunately, resistance to BTK and BCL2 inhibitors occurs, indicating the need for novel approaches and combinations (2, 3, 11-14).

Small-molecule BTK protein degraders are a novel class of anti-lymphoma agents with promising preclinical and early clinical data (4, 15-22). Among these, tacabrutideg (BGB-16673) is an orally available chimeric degradation-activating compound (CDAC), inducing the cereblon-mediated degradation of BTK (15, 20, 23). It the phase 1 trial for patients with R/R B cell lymphomas, including MZL patients, tacabrutideg has shown a promising activity (ORR of 50%, n.=20) and tolerable safety (23-25). It is currently in phase 3 trials for patients with R/R chronic lymphocytic leukemia (CLL) (NCT06973187, NCT06970743, NCT06846671).

Venetoclax, the first-in-class specific inhibitor of BCL2, is currently approved for treating CLL and MCL, while its use in MZL remains investigational despite promising preclinical and early clinical data. Sonrotoclax (BGB-11417) is a second-generation BCL2 inhibitor with reported more robust preclinical anti-tumor activity than venetoclax in a few models derived from mantle cell lymphoma (MCL) and diffuse large B-cell lymphoma (26-28). In an ongoing phase 1 trial, the preliminary results show an ORR of 67% and 33% complete responses in 12 R/R MZL patients (29). Sonrotoclax is currently in Phase 3 trials for patients with R/R MCL or CLL, and in the first-line setting for CLL patients (NCT06073821, NCT06943872, NCT06742996).

Here, we assessed the BTK degrader tacabrutideg in models derived from bona fide MZL, including some in which we have induced secondary resistance to BTK and PI3K inhibitors (3, 12, 30-32), as a single agent and in combination with other molecules, including the two BCL2 inhibitors venetoclax and sonrotoclax, to provide the rationale for future trials in MZL patients.

Methods

Cell lines

VL51, SSK41, Karpas1718, HC1, ESKOL, HAIRM, REC1, and MINO cells were cultured under recommended conditions, supplemented with 10–20% fetal bovine serum and penicillin–streptomycin–neomycin (Sigma). Cell line identity was verified by short tandem repeat profiling (Promega GenePrint 10 System), and mycoplasma contamination was routinely excluded (MycoAlert, Lonza).

Resistant cell lines

Previously in-house-developed derivatives of the VL51, Karpas1718, and SSK41 cell lines with secondary resistance to BTK (32), PI3K (3, 12, 30), and BCL2 (31, 33) inhibitors were tested for sensitivity to tacabrutideg as a single agent.

Compounds and cytotoxicity assays

Tacabrutideg, BGB-21704, and sonrotoclax were provided by Beigene. Venetoclax, zanubrutinib, bendamustine, selinexor, lenalidomide, and tazemetostat were purchased from Selleckchem; rituximab was obtained from Roche. Cells (2×10^4/well) were exposed to compounds alone or in combination for 5 days and viability assessed by MTT assay. A 5-day exposure was selected to capture both early and delayed biological effects of BTK targeting, including cumulative cytostatic and apoptotic responses, while minimizing variability associated with prolonged culture conditions. IC_{50} values were calculated by four-parameter logistic regression (PharmacoGx), and drug

interactions were evaluated using the Highest Single Agent (HSA) model implemented in SynergyFinder Plus. Drug concentrations are listed in Supplementary Table S1.

Immunoblotting

Cells were treated for 24 hours, lysed in M-PER buffer supplemented with protease and phosphatase inhibitors, and analyzed by SDS-PAGE and immunoblotting. Antibodies against BTK, p-BTK (Y223), PLCG2, p-PLCG2 (Y1217), ERK, p-ERK (T202/Y204), BCL2, MCL1, BCL-XL, GAPDH, and vinculin were obtained from Cell Signaling Technology or eBioscience. Signals were detected by enhanced chemiluminescence and quantified using a Fusion Solo S instrument.

Apoptosis and proliferation assays.

Apoptosis was assessed by Annexin V/propidium iodide staining and flow cytometry. For real-time proliferation analyses, VL51 and Karpas1718 cells were monitored for 5 days using the IncuCyte platform following treatment with DMSO, tacabrutideg, zanubrutinib, sonrotoclax, or the tacabrutideg/sonrotoclax combination. Growth curves and area-under-the-curve values were generated from confluence measurements.

Three-dimensional co-culture and primary samples

VL51, Karpas1718, and SSK41 cells stably expressing mCherry were cultured in a three-dimensional co-culture system with human bone marrow stromal cells and exposed to the indicated treatments. Detailed procedures are provided in the Supplementary Methods.

Primary MZL cells (n=3; one splenic and two nodal MZL) were treated with tacabrutideg and monitored by IncuCyte imaging for 72 hours. Surface CD20 expression was confirmed by flow cytometry, and intracellular p-ERK (T202/Y204) was assessed by flow cytometry after 24 hours of tacabrutideg treatment. All studies were conducted in accordance with applicable ethical regulations.

RNA sequencing and bioinformatics

RNA libraries were prepared using the NEBNext Ultra Directional kit and sequenced on a NextSeq 2000 platform. Reads were quality-controlled, trimmed, aligned to hg38 (STAR), and quantified using HTSeq-count. Differential expression analysis was performed using edgeR/voom, and gene set enrichment analyses were conducted with MSigDB and SignatureDB. Data are available under GEO accession GSE312595.

Molecular docking

Tacabrutideg structures were generated from SMILES, protonated, and prepared using OpenBabel, MolGpKa, and UCSF Chimera. Docking to BTK was performed with AutoDock 4.2 using the Lamarckian Genetic Algorithm, and binding poses were visualized in Chimera.

Results

The BTK-degrader tacabrutideg has single-agent activity in individual MZL.

The effect of the BTK-degrader tacabrutideg on cell viability was assessed after five days of exposure in six MZL cell lines, plus two BTK inhibitor-sensitive MCL cell lines, which we included as positive controls (Figure 1A; Supplementary Table S2). The SSK41 and Karpas1718 were highly sensitive, with IC50 values of 0.27 and 1.89 nM, respectively (Figure 1). A minor response was observed in the MZL VL51 cell line. No effect was observed in the remaining three MZL models (HC1, HAIRM, and ESKOL) with concentrations of tacabrutideg up to 10 μM. Tacabrutideg was also very active in the two MCL cell lines: REC1 (IC50 0.001 nM) and MINO (0.03 nM) (Figure 1A; Supplementary Table S2). In the two sensitive MZL cell lines, tacabrutideg and zanubrutinib exerted comparable effects on cell viability as measured by MTT assay (Figure 1B, Supplementary Figure 1B). However, real-time monitoring of cell proliferation revealed that tacabrutideg induced a more pronounced inhibition of cell growth than zanubrutinib in the sensitive Karpas1718 model (Figure 1C). Notably, although VL51 cells displayed only a limited response in the metabolic viability assay, continuous IncuCyte monitoring demonstrated a significant reduction in cell growth following exposure to tacabrutideg at concentrations below 1 μM. A similar, albeit slightly less pronounced, effect was observed with zanubrutinib (Figure 1D). These findings suggest that conventional

endpoint viability assays may underestimate the biological activity of BTK-targeting agents in selected MZL models.
A lower response was observed with BGB-21704, a compound similar to tacabrutideg but without BTK-related activity, compared to the BTK degrader (Supplementary Figure 3).
Reduced activity was observed in a panel of cell lines derived from the VL51, Karpas1718, and SSK41, which exhibited secondary resistance to BTK, PI3K, and BCL2 inhibitors (3, 12, 30-33) (Supplementary Figure 4).

The BTK-degrader tacabrutideg and the BTK inhibitor zanubrutinib induce similar transcriptomic changes in MZL cell lines.
To compare the mechanism of action between the BTK degrader and the BTK inhibitor, we performed RNA-Seq on RNA extracted from the Karpas1718 cell line exposed to tacabrutideg (5 nM), zanubrutinib (5 nM), or, as a control, to DMSO for 8, 12, and 24 hours (Supplementary Table S3). The effect of the two compounds on the cell line was very similar (Figure 2A, Supplementary Figure 5A, $r=0.58$, $P < 0.001$). Both agents downregulated key gene sets, including NF-κB and B cell receptor signaling, and showed overlapping signatures with other BTK-targeting compounds (Figure 2B). Although still of potential interest for combination studies, only tacabrutideg appeared to downregulate the ribosome machinery, transcripts involved in oxidative phosphorylation, and genes repressed by anti-CD20 therapies. Conversely, zanubrutinib seemed to repress DNA damage transcripts and essential and mutated genes in DLBCL (Supplementary Figure 5B-D).
Both zanubrutinib and tacabrutideg down-regulated the levels of p-BTK(Tyr223), but only the latter down-regulated the total BTK protein levels in all six MZL cell lines (Figure 3, Supplementary Figure 2). The effect followed different kinetics, but overall BTK expression did not appear to be a major determinant of response. However, upon exposure to tacabrutideg, resistant lines retained significantly higher levels of phosphorylated BTK (p-BTK), either p-BTK alone ($p=0.044$) or the p-BTK/BTK ratio ($p=0.042$), compared to sensitive lines (Supplementary Figure 2G), suggesting that resistant cells maintain active BTK signaling despite drug exposure.
To more accurately assess BCR pathway inhibition in the context of BTK degradation, we evaluated downstream signaling components. Tacabrutideg induced a consistent reduction of p-PLCG2 and p-ERK levels across MZL models, supporting effective functional suppression of BCR signaling (Figure 3, Supplementary Figure 2).

The BTK-degrader tacabrutideg synergizes with other targeted agents in MZL cell lines.
To explore the potential benefits of tacabrutideg-based combinations, we exposed four MZL cell lines to increasing concentrations of the BTK degrader and a series of agents used in clinical settings or in clinical development for 5 days. The BTK degrader was combined with the two BCL2 inhibitors venetoclax and sonrotoclax, the cereblon E3 ligase modulator lenalidomide, the XPO1 inhibitor selinexor, the EZH2 inhibitor tazemetostat, the DNA alkylating agent bendamustine, and the CD20 targeting monoclonal antibody rituximab (Table 1; Supplementary Figure 6). Considering additivity and synergism, most combinations were beneficial across the cell lines. The best results were obtained when we combined tacabrutideg with the BCL2 inhibitors venetoclax or Sonrotoclax (Figure 4A) and, to a lesser extent, with bendamustine, lenalidomide, and rituximab (Supplementary Figure 6). Thus, considering the clinical potential, we then focused on combining tacabrutideg and sonrotoclax to better understand the mechanisms underlying the observed synergy.
When we assessed apoptosis induction after 24 hours of exposure to tacabrutideg as a single agent or in combination with venetoclax, sonrotoclax, or bendamustine, we observed higher apoptosis with the combinations than with the single agents (Supplementary Figure 7). To complement endpoint viability and apoptosis assays, one sensitive (Karpas1718) and one resistant (VL51) cell line were monitored by live-cell imaging during exposure to tacabrutideg, sonrotoclax, or the tacabrutideg/sonrotoclax combination. In VL51 cells, single agents produced modest growth inhibition, whereas the combination more consistently reduced cell expansion over time. In Karpas1718 cells, tacabrutideg and sonrotoclax showed marked single-agent activity, and the combination further constrained cell growth, as reflected by growth curves and area-under-the-

curve quantification. These results support the anti-proliferative activity of the BTK degrader and its combination with sonrotoclax beyond conventional endpoint viability assays (Figure 4B).
We next investigated the changes in protein levels of p-BTK(Tyr223)/BTK, BCL2, MCL1, and BCL-XL in VL51 and Karpas1718 MZL models. The exposure to tacabrutideg decreased total BTK and p-BTK(Tyr223) levels in both cell lines. The effect was maintained in cells exposed to both tacabrutideg and sonrotoclax (Figure 4C, Supplementary Figure 8). Both Karpas1718 and VL51 cells showed upregulation of BCL2 after exposure to the lower concentration of the BTK degrader (0.5 nM) as a single agent or in combination with sonrotoclax. No changes were observed when cells were exposed to 1 nM of tacabrutideg, either alone or in combination (Figure 4C, Supplementary Figure 8). Sonrotoclax, as a single agent, increased MCL1 levels in VL51 cells, with a slight increase in Karpas1718 cells. On the other hand, the BTK degrader tacabrutideg repressed MCL1 in Karpas1718 when given as a single agent and in combination with sonrotoclax. In VL51 cells, the BTK degrader up-regulated MCL1 at 1 μM with no effect at lower doses. Finally, the BTK degrader downmodulated BCL-XL in Karpas1718 but not in VL51 (Figure 4C, Supplementary Figure 8).

The BCL2 inhibitor sonrotoclax is more active than venetoclax in MZL models.
The combination experiments also allowed a direct comparison between the first- and second-generation BCL2 inhibitors in four cell lines: sonrotoclax was over ten times more active than venetoclax in three cell lines (HC1, HAIRM and Karpas1718), showed improved activity at low doses in models (VL51 and ESKOL, and equally active in the remaining cell line (SSK41) (Supplementary Figure 9; Supplementary Table S4).

Tacabrutideg and sonrotoclax retain activity in a three-dimensional stromal co-culture model.
To evaluate the activity of the drugs in a microenvironment-mimicking context, we tested tacabrutideg, zanubrutinib, sonrotoclax, and the tacabrutideg/sonrotoclax combination in a three-dimensional co-culture system with human bone marrow stromal cells. Stromal support allowed lymphoma cell growth in control conditions. Across VL51, Karpas1718, and SSK41 cells, tacabrutideg retained anti-lymphoma activity, and the combination with sonrotoclax showed the most consistent growth inhibition, partially overcoming stromal-mediated protection (Figure 5; Supplementary Figure 10). These findings extend the 2D cytotoxicity data and support the activity of dual BTK/BCL2 targeting in a more physiologically relevant setting.

Tacabrutideg inhibits ERK phosphorylation and reduces growth in primary MZL samples.
We next explored the activity of tacabrutideg in primary MZL samples from three patients, including one splenic MZL and two nodal MZL cases. IncuCyte monitoring showed a reduction in cell growth following exposure to tacabrutideg, with variable magnitude across samples and concentrations. In parallel, phospho-flow analysis after 24 hours demonstrated reduced intracellular p-ERK levels in CD20-positive primary cells exposed to tacabrutideg (Figure 6). These data provide patient-derived evidence that BTK degradation can suppress downstream BCR signaling and limit growth in primary MZL cells.

The binding mode of tacabrutideg to BTK.
We elucidated the binding mode of tacabrutideg to BTK via docking calculations, which is a widely employed technique to study ligand/protein binding interactions (34-37). We first investigated the binding of TACABRUTIDEG to the kinase domain of human BTK (UniProt ID: Q06187, residues 395–656), taking advantage of the reported crystallographic atomic structure of the protein in complex with the BTK inhibitor 4-~{tert}-butyl-~{N}-[2-methyl-3-[6-[4-(4-methylpiperazin-1-yl)carbonylphenyl]-7~(38)-pyrrolo[2,3-d]pyrimidin-4-yl]phenyl]benzamide (39), which we refer to hereafter as L0Z (PDB ID: 6S90). Among the top-scoring docking poses, tacabrutideg occupied the BTK active site in a conformation highly similar to that of zanubrutinib and closely resembling the crystallographic binding mode of the BTK inhibitor L0Z (Supplementary Figure 11A-B). The binding

poses of tacabrutideg and L0Z showed a low root-mean-square deviation (r.m.s.d.) of 0.8 Å across their conserved scaffolds. In both compounds, the tert-butyl group occupies a hydrophobic pocket formed by residues including PHE413, LEU542, and VAL546, while the pyrrolopyrimidine core establishes hydrogen bonds with the backbone of MET477. Tacabrutideg further forms hydrogen bonds with LYS430 and ASN526 and, unlike L0Z, establishes an additional salt bridge between its piperazine moiety and GLU488. The terminal region of tacabrutideg may also interact with ARG490 and HIS491, potentially stabilizing the binding mode. A superposition of the binding conformations of tacabrutideg and L0Z is shown in Supplementary Figure 11D.
Notably, the clinically relevant A428D mutation, reported in lymphoma cell lines resistant to both covalent and non-covalent BTK inhibitors, lies within the BTK ATP-binding site, at the interface with tacabrutideg (40). Substitution of alanine with aspartic acid introduces a longer, negatively charged side chain in place of a small hydrophobic residue, markedly altering both the shape and physicochemical properties of the binding pocket. In particular, in A428D-BTK, the aspartate side chain may sterically hinder ligand accommodation and create an unfavorable electrostatic interaction with the lone pair of the pyrrolopyrimidine nitrogen positioned near the mutated residue. These effects are predicted to weaken ligand binding and may help explain the resistance of A428D-BTK to tacabrutideg (Supplementary Figure 11C). In addition, A428D may induce a conformational rearrangement of the activation loop, causing it to extend into the binding pocket and clash with ligands accessing this region, as proposed by *Sievers et al.* (41).

Discussion

Here, we provide a comprehensive preclinical evaluation of BTK degradation in MZL and demonstrate that tacabrutideg exerts anti-lymphoma activity as a single agent and synergizes with several targeted therapies, most notably the BCL2 inhibitor sonrotoclax. Although the transcriptional and functional effects of tacabrutideg largely recapitulated those of zanubrutinib, BTK degradation resulted in sustained suppression of downstream signaling and robust anti-proliferative activity. We additionally show that sonrotoclax is more potent than venetoclax in MZL models and markedly enhances the activity of tacabrutideg. Importantly, these effects were preserved in a stromal-supported 3D co-culture system and validated in primary MZL samples, in which tacabrutideg reduced cell growth and inhibited ERK signaling. Collectively, these findings provide strong biological support for the clinical development of BTK degrader–based strategies, particularly in combination with next-generation BCL2 inhibitors, in patients with MZL.

The BTK degrader tacabrutideg showed potent single-agent activity, particularly low IC50 values, in two MZL and two MCL cell lines. These findings are consistent with the essential role of BTK in B-cell malignancies (1, 2, 42, 43). They also underscore the efficacy of targeted BTK degradation as a therapeutic strategy, which is now undergoing early clinical evaluation (4, 16, 19, 21, 22, 44). In the MZL models evaluated here, BTK degradation and covalent BTK inhibition produced largely overlapping biological effects, indicating that tacabrutideg preserves the pathway specificity of BTK-directed therapies. However, BTK degradation resulted in complete target removal and distinct transcriptional changes, including repression of oxidative phosphorylation programs, which may contribute to improved disease control and resistance prevention.
The limited sensitivity of VL51, HC1, HAIRM, and ESKOL cells may reflect reduced dependence on BTK/BCR signaling and activation of compensatory pathways. Consistent with this hypothesis, some models retained residual BTK and downstream signaling despite efficient BTK degradation. Notably, although VL51 cells showed limited sensitivity in metabolic viability assays, real-time monitoring revealed significant growth inhibition following tacabrutideg exposure, suggesting that BTK degradation predominantly exerts cytostatic effects in certain MZL models. Together, these findings highlight the biological heterogeneity of MZL and suggest that alternative signaling networks may sustain survival while only partially preserving proliferation.
Because BTK degraders deplete total BTK protein, p-BTK/BTK ratios should be interpreted with caution. Accordingly, downstream signaling nodes provide more informative pharmacodynamic readouts of BTK activity. Tacabrutideg consistently suppressed PLCG2 and ERK phosphorylation in both sensitive and intrinsically resistant MZL models, while inhibition of ERK phosphorylation

was also confirmed in *ex vivo* primary MZL cells, demonstrating effective suppression of downstream BCR signaling.

The effect on p-BTK inhibition was comparable, despite the fact that the degradation of the whole protein was exclusively induced by tacabrutideg and not by zanubrutinib. We cannot exclude that the latter phenomenon might differentiate the activity degrader from the inhibitors in other experimental settings in the clinical context. Indeed, in line with this, RNA-Seq analysis revealed substantial overlap in the transcriptomic changes induced by tacabrutideg and zanubrutinib, while pinpointing possible differences between the two compounds. The significant downregulation of MYC targets and B-cell receptor signaling genes underscores the shared pathways targeted by BTK inhibition and degradation in these cellular models. Tacabrutideg uniquely downregulated transcripts involved in oxidative phosphorylation, which could be a potential differentiator in its mechanism of action and therapeutic effect. Notably, oxidative phosphorylation is a metabolic process that we and others have associated with resistance to anti-cancer agents, including BTK inhibitors (45-49). This effect, along with the removal of the entire protein, might reduce the risk of resistance compared to BTK inhibitors when lymphoma cells are exposed to the compounds for a long time. However, this must be validated in future preclinical and clinical studies.

Molecular docking studies further showed that tacabrutideg occupies the BTK active site similarly to zanubrutinib, adopting a binding mode closely resembling the reported crystallographic binding mode of the non-covalent selective inhibitor L0Z (39).

Preclinical evidence indicates that tacabrutideg and other BTK-degraders in clinical development can overcome the resistance driven by BTK mutations (17, 18, 20, 50, 51). Interestingly, Montoya et al. demonstrated that the BTK and IKZF1/3 degrader NX-2127 can also counteract the oncogenic scaffold function of mutant BTK proteins, which activate additional kinases such as HCK and ILK, contributing to resistance against BTK inhibitors (44). We also tested tacabrutideg in the MZL model, which does not bear *BTK* mutations, with secondary resistance to BTK or PI3K inhibitors (3, 12, 30-33). The tacabrutideg activity was reduced in this model, suggesting that BTK does not serve as a scaffold to sustain active signaling cascades that support resistance in these models.

The synergistic potential of tacabrutideg was especially evident when combined with other agents like BCL2 inhibitors (venetoclax and sonrotoclax), lenalidomide, rituximab, and bendamustine. This combination led to an enhanced apoptotic response, indicating a promising strategy for combination therapies with tacabrutideg in MZL. The benefit of combining tacabrutideg with lenalidomide is particularly noteworthy, as both agents utilize cereblon to degrade their targets (28, 52). To improve the physiological relevance of our results, we tested tacabrutideg alone and with sonrotoclax in a 3D co-culture system with bone marrow stromal cells. In this setup, the combination maintained significant anti-tumor activity and partially countered stromal-mediated protection, suggesting its potential effectiveness within the tumor microenvironment. Although the tacabrutideg activity was confirmed in stromal-supported co-cultures and primary MZL samples, future research using patient-derived xenografts and other clinically relevant models will be crucial to validate these findings.

The superior efficacy of sonrotoclax, a second-generation BCL2 inhibitor with reported more robust preclinical anti-tumor activity in a few models derived from MCL and diffuse large B cell lymphoma (26), over the first-generation BCL2 inhibitor venetoclax in certain cell lines is particularly noteworthy, suggesting it is a potent agent in MZL as a single agent or a partner in combination regimens. Indeed, despite the promising results achieved with a manageable safety profile and durable responses in a subset of patients treated with venetoclax (5), BCL2 inhibitors have not been exploited in MZL patients so far. Our data show higher activity than venetoclax in MZL models, and the early results from the ongoing phase 1 trials in patients with MZL (29) or Waldenström's macroglobulinemia (53) strongly support the clinical development of this agent for MZL patients, as a single or in combination. The preliminary results reported for 14 R/R MZL patients enrolled in a phase 2 study combining ibrutinib and venetoclax support the dual BTK and BCL2 inhibition for this disease as a safe and active regimen with a complete remission rate of 43% according to PET/CT response at week 56 (9, 10). Data obtained in patients with chronic lymphocytic leukemia indicate that also combining sonrotoclax and zanubrutinib also seems safe (54). No data are available on

sonrotoclax combined with BTK degraders, but the ongoing trial NCT06634589 is exploring the combination of sonrotoclax and tacabrutideg in patients with R/R B-cell lymphomas.

Our findings further support the potent and selective activity of tacabrutideg in MZL and MCL models. Beyond inducing BTK degradation, tacabrutideg suppressed downstream BCR signaling, reduced lymphoma cell growth in established cell lines and primary MZL samples, and retained activity in a stromal-supported microenvironment. Moreover, its robust synergy with several clinically relevant agents, particularly the second-generation BCL2 inhibitor sonrotoclax, highlights the therapeutic potential of combining BTK degradation with complementary inhibition of survival pathways. Notably, sonrotoclax demonstrated greater anti-lymphoma activity than venetoclax across multiple MZL models.

Collectively, these results provide a strong biological and translational rationale for the clinical development of BTK degrader–based strategies in MZL. In particular, the combination of tacabrutideg and sonrotoclax emerges as a promising approach that simultaneously targets BCR signaling and apoptotic dependency, two key vulnerabilities of malignant B cells. Ongoing clinical studies will determine whether the encouraging preclinical activity observed here translates into meaningful clinical benefit for patients with MZL.

References

1. McDonald C, Xanthopoulos C, Kostareli E. The role of Bruton's tyrosine kinase in the immune system and disease. Immunology. 2021;164(4):722-736.

2. Stephens DM, Byrd JC. Resistance to Bruton tyrosine kinase inhibitors: the Achilles heel of their success story in lymphoid malignancies. Blood. 2021;138(13):1099-1109.

3. Arribas AJ, Napoli S, Cascione L, et al. Resistance to PI3Kdelta inhibitors in marginal zone lymphoma can be reverted by targeting the IL-6/PDGFRA axis. Haematologica. 2022;107(11):2685-2697.

4. Tam CS, Frustaci AM, Bijou F, et al. Preliminary efficacy and safety of the bruton tyrosine kinase degrader BGB-16673 in patients with relapsed or refractory (R/R) indolent NHL: results from the phase 1 CaDAnCe-101 study. Blood. 2024;144(Supplement 1):1649.

5. Davids MS, Roberts AW, Kenkre VP, et al. Long-term follow-up of patients with relapsed or refractory Non-Hodgkin lymphoma treated with venetoclax in a phase I, first-in-human study. Clin Cancer Res. 2021;27(17):4690-4695.

6. Noy A, de Vos S, Thieblemont C, et al. Targeting Bruton tyrosine kinase with ibrutinib in relapsed/refractory marginal zone lymphoma. Blood. 2017;129(16):2224-2232.

7. Opat S, Tedeschi A, Hu B, et al. Safety and efficacy of zanubrutinib in relapsed/refractory marginal zone lymphoma: final analysis of the MAGNOLIA study. Blood Adv. 2023;7(22):6801-6811.

8. Deng L, Li Z, Zhang H, et al. Orelabrutinib for the treatment of relapsed or refractory marginal zone lymphoma: A phase 2, multicenter, open-label study. Am J Hematol. 2023;98(11):1742-1750.

9. Handunnetti SM, Khot A, Anderson MA, et al. Safety and efficacy of ibrutinib in combination with venetoclax in patients with marginal zone lymphoma: preliminary results from an open label, phase II study. Blood. 2019;134(Supplement_1):3999.

10. Davis JE, Le LH, Ludford-Menting M, et al. Marginal zone lymphoma is associated with dysregulated peripheral blood immunity which is not changed by ibrutinib-venetoclax treatment. Blood. 2024;144(Supplement 1):4384.

11. Nakhoda S, Vistarop A, Wang YL. Resistance to Bruton tyrosine kinase inhibition in chronic lymphocytic leukaemia and non-Hodgkin lymphoma. Br J Haematol. 2023;200(2):137-149.

12. Arribas AJ, Napoli S, Cascione L, et al. ERBB4-mediated signaling is a mediator of resistance to PI3K and BTK Inhibitors in B-cell lymphoid neoplasms. Mol Cancer Ther. 2024;23(3):368-380.

13. Stephens DM, Byrd JC. Next-generation bruton tyrosine kinase inhibitors. J Clin Oncol. 2020;38(25):2937-2940.

14. Lue JK, O'Connor OA, Bertoni F. Targeting pathogenic mechanisms in marginal zone lymphoma: from concepts and beyond. Ann Lymphoma. 2020;4:7.

15. Feng X, Wang Y, Long T, et al. P1239: Bruton tyrosine kinase (BTK) protein degrader BGB-16673 is less apt to cause, and able to overcome variable BTK resistance mutations compared to other BTK inhibitors (BTKi). Hemasphere. 2023;7(Suppl):e368855c.

16. Danilov A, Tees MT, Patel K, et al. A first-in-human phase 1 trial of NX-2127, a first-in-class Bruton's Tyrosine Kinase (BTK) dual-targeted protein degrader with immunomodulatory activity, in patients with relapsed/refractory B cell malignancies. Blood. 2023;142(Supplement 1):4463-4463.

17. Robbins DW, Noviski MA, Tan YS, et al. Discovery and preclinical pharmacology of NX-2127, an orally bioavailable degrader of Bruton's tyrosine kinase with immunomodulatory activity for the treatment of patients with B cell malignancies. J Med Chem. 2024;67(4):2321-2336.

18. Noviski MA, Brathaban N, Mukerji R, et al. Abstract 2850: NX-5948 promotes selective, sub-nanomolar degradation of inhibitor-resistant BTK mutants. Cancer Res. 2023;83(7_Supplement):2850.

19. Searle E, Forconi F, Linton K, et al. Initial FindinGS FROM A FIRST-IN-HUMAN PHASE 1a/b trial of NX-5948, a selective bruton's tyrosine kinase (BTK) degrader, in patients with relapsed/refractory B cell malignancies. Blood. 2023;142(Supplement 1):4473.

20. Wang H, Hou X, Zhang W, et al. P1219: BGB-16673, a BTK degrader, overcomes on-target resistance from BTK inhibitors and presents sustainable long-term tumor regression in lymphoma xenograft models. Hemasphere. 2023;7(Suppl):e24358c2.

21. Seymour JF, Tam CS, Cheah CY, et al. Preliminary efficacy and safety of the bruton tyrosine kinase degrader BGB-16673 in patients with relapsed or refractory waldenström macroglobulinemia: results from the phase 1 CaDAnCe-101 Study. Blood. 2024;144(Supplement 1):860.

22. Shah NN, Omer Z, Collins GP, et al. Efficacy and safety of the Bruton's tyrosine kinase (BTK) degrader NX-5948 in patients with relapsed/refractory (R/R) chronic lymphocytic leukemia (CLL): updated results from an ongoing phase 1a/b study. Blood. 2024;144(Supplement 1):884.

23. Seymour JF, Cheah CY, Parrondo R, et al. First results from a phase 1, first-in-human study of the Bruton's tyrosine kinase (BTK) degrader Bgb-16673 in patients (Pts) with relapsed or refractory (R/R) B-cell malignancies (BGB-16673-101). Blood. 2023;142(Supplement 1):4401.

24. Tam C, Thompson PA. BTK inhibitors in CLL: second-generation drugs and beyond. Blood Adv. 2024;8(9):2300-2309.

25. Zinzani PL, Frustaci AM, Narkhede M, et al. Updated efficacy/safety of bruton tyrosine kinase degrader BGB-16673 in patients with relapsed/refractory indolent NHL: ongoing phase 1 CaDAnCe-101 RESULTS. Hematol Oncol. 2025;43(S3):e436_70094.

26. Liu J, Li S, Wang Q, et al. Sonrotoclax overcomes BCL2 G101V mutation-induced venetoclax resistance in preclinical models of hematologic malignancy. Blood. 2024;143(18):1825-1836.

27. Guo Y, Xue H, Hu N, et al. Discovery of the clinical candidate sonrotoclax (BGB-11417), a highly potent and selective inhibitor for both WT and G101V mutant Bcl-2. J Med Chem. 2024;67(10):7836-7858.

28. Wu Y, Meibohm B, Zhang T, et al. Translational modelling to predict human pharmacokinetics and pharmacodynamics of a Bruton's tyrosine kinase-targeted protein degrader BGB-16673. Br J Pharmacol. 2024;181(24):4973-4987.

29. Tedeschi A, Cheah CY, Opat SS, et al. Monotherapy with second-generation BCL2 inhibitor sonrotoclax (BGB-11417) is well tolerated with high response rates in patients with relapsed/refractory marginal zone lymphoma: data from an ongoing phase 1 study. Blood. 2023;142(Supplement 1):3032.

30. Arribas A, Napoli S, Cascione L, et al. Secondary resistance to the PI3K inhibitor copanlisib in marginal zone lymphoma. Eur J Cancer. 2020;138:S40.

31. Arribas AJ, Cascione L, Cannas E, et al. Abstract 534: Novel marginal zone lymphoma models of resistance to the dual inhibition of PI3K and BCL2. Cancer Res. 2024;84(6_Supplement):534.

32. Arribas AJ, Cannas E, Sartori G, et al. IL-16 production is a mechanism of resistance to BTK inhibitors and R-CHOP in lymphomas. Blood. 2026;148(10):1312-1327.

33. Arribas AJ, Fuzio F, Cannas E, et al. Abstract 1848: IL-1-driven signaling promotes resistance to PI3K and BCL2 inhibitors in B-cell lymphoma preclinical models. Cancer Res. 2026;86(7_Supplement):1848.

34. Limongelli V. Ligand binding free energy and kinetics calculation in 2020. Wires Comput Mol Sci. 2020;10(4):e1455.

35. Di Leva FS, Di Marino D, Limongelli V. Structural insight into the binding mode of FXR and GPBAR1 modulators. Handb Exp Pharmacol. 2019;256:111-136.

36. Heckmann D, Laufer B, Marinelli L, et al. Breaking the dogma of the metal-coordinating carboxylate group in integrin ligands: introducing hydroxamic acids to the MIDAS to tune potency and selectivity. Angew Chem Int Ed Engl. 2009;48(24):4436-4440.

37. Carino A, Biagioli M, Marchiano S, et al. Disruption of TFGbeta-SMAD3 pathway by the nuclear receptor SHP mediates the antifibrotic activities of BAR704, a novel highly selective FXR ligand. Pharmacol Res. 2018;131:17-31.

38. Anders S, Pyl PT, Huber W. HTSeq--a Python framework to work with high-throughput sequencing data. Bioinformatics. 2015;31(2):166-169.

39. Pulz R, Angst D, Dawson J, et al. Design of potent and selective covalent inhibitors of Bruton's tyrosine kinase targeting an inactive conformation. ACS Med Chem Lett. 2019;10(10):1467-1472.

40. Wong RL, Choi MY, Wang HY, et al. Mutation in Bruton Tyrosine Kinase (BTK) A428D confers resistance To BTK-degrader therapy in chronic lymphocytic leukemia. Leukemia. 2024;38(8):1818-1821.

41. Sievers Q, Lu H, Cool A, et al. Molecular and structural basis of pan-resistance to BTK targeting therapies via BTK A428D mutation. Blood. 2025;146(Supplement 1):2102.

42. Bonfiglio F, Bruscaggin A, Guidetti F, et al. Genetic and phenotypic attributes of splenic marginal zone lymphoma. Blood. 2022;139(5):732-747.

43. Rossi D, Bertoni F, Zucca E. Marginal-zone lymphomas. N Engl J Med. 2022;386(6):568-581.

44. Montoya S, Bourcier J, Noviski M, et al. Kinase-impaired BTK mutations are susceptible to clinical-stage BTK and IKZF1/3 degrader NX-2127. Science. 2024;383(6682):eadi5798.

45. Zhao Z, Mei Y, Wang Z, et al. The effect of oxidative phosphorylation on cancer drug resistance. Cancers (Basel). 2022;15(1):62.

46. Tarantelli C, Gaudio E, Arribas AJ, et al. PQR309 is a novel dual PI3K/mTOR inhibitor with preclinical antitumor activity in lymphomas as a single agent and in combination therapy. Clin Cancer Res. 2018;24(1):120-129.

47. Liu Y, Kimpara S, Hoang NM, et al. EGR1-mediated metabolic reprogramming to oxidative phosphorylation contributes to ibrutinib resistance in B-cell lymphoma. Blood. 2023;142(22):1879-1894.

48. Zammarchi F, Havenith KE, Sachini N, et al. ADCT-602, a novel PBD dimer-containing antibody-drug conjugate for treating CD22-positive hematologic malignancies. Mol Cancer Ther. 2024;23(4):520-531.

49. Mensah AA, Spriano F, Sartori G, et al. Study of the antilymphoma activity of pracinostat reveals different sensitivities of DLBCL cells to HDAC inhibitors. Blood Adv. 2021;5(10):2467-2480.

50. Pan C, Riehm J, Gururaja TL, et al. Abstract 605: ABBV-101, a highly potent and selective clinical stage Bruton tyrosine kinase degrader, overcomes BTK mutation-induced resistance to BTK inhibitors. Cancer Res. 2024;84(6_Supplement):605.

51. Li J, Xu W, Yan P, et al. Abstract CT128: Phase 1 study of HSK29116, a Bruton tyrosine kinase (BTK) proteolysis-targeting chimera (PROTAC) agent, in patients with relapsed or refractory B-cell malignancies. Cancer Res. 2023;83(8_Supplement):CT128.

52. Lopez-Girona A, Mendy D, Ito T, et al. Cereblon is a direct protein target for immunomodulatory and antiproliferative activities of lenalidomide and pomalidomide. Leukemia. 2012;26(11):2326-2335.

53. Cheah C, Tam C, Sanz RG, et al. P1110: Safety and efficacy results of a phase 1 study of the novel BCL2 inhibitor sonrotoclax (BGB-11417) for relapsed/refractory Waldenström's macroglobulinemia. Hemasphere. 2024;8(S1):2017-2018.

54. Soumerai JD, Cheah CY, Anderson MA, et al. Sonrotoclax and zanubrutinib as frontline treatment for CLL demonstrates high MRD clearance rates with good tolerability: data from an ongoing phase 1/1b study BGB-11417-101. Blood. 2024;144(Supplement 1):1012.

Tables

Table 1. Tacabrutideg-based combinations in four MZL lymphoma cell lines. Results were obtained via MTT after five days of exposure. HSA, highest single agent.

Drug	Mechanism of action	Cell line	Synergy score (HSA)	Effect
Lenalidomide	cereblon E3 ligase modulator	Karpas1718	6.5	Additivity
		HC1	2.67	Additivity
		SSK41	11.38	Synergy
		VL51	4.84	Additivity
Selinexor	XPO1 inhibitor	Karpas1718	-17.28	Antagonism
		HC1	3.69	Additivity
		SSK41	13.57	Synergy
		VL51	8.98	Additivity
Venetoclax	First-generation BCL2 inhibitor	Karpas1718	4.65	Additivity
		HC1	3.41	Additivity
		SSK41	4.07	Additivity
		VL51	14.5	Synergy
Sonrotoclax	Second-generation BCL2 inhibitor	Karpas1718	6.62	Additivity
		HC1	1.19	Additivity
		SSK41	5.73	Additivity
		VL51	15.76	Synergy
Bendamustine	DNA alkylating agent	Karpas1718	9.07	Additivity
		HC1	3.18	Additivity
		SSK41	2.19	Additivity
		VL51	7.82	Additivity
Tazemetostat	EZH2 inhibitor	Karpas1718	-7.81	Antagonism
		HC1	4.42	Additivity
		SSK41	11.8	Synergy
		VL51	6.5	Additivity
Rituximab	CD20 targeting monoclonal antibody	Karpas1718	1.34	Additivity
		HC1	3.27	Additivity
		SSK41	6.63	Additivity
		VL51	14.17	Synergy

Figure Legends

Figure 1. Pharmacological profiles of the BTK-degrader tacabrutideg and the BTK inhibitor zanubrutinib in marginal zone lymphoma cells.
Effect on cell viability (MTT assay) of five days of exposure to the BTK-degrader tacabrutideg (A) or to the BTK inhibitor zanubrutinib (B) in cell lines derived from MZL (VL51, SSK41, Karpas1718, HC1, HAIRM, ESKOL) and from MCL (REC1, MINO). Error bars correspond to the SD.
(C–D) Karpas1718 (C) and VL51 (D) cells were cultured in the presence of the indicated treatments and monitored continuously for 5 days using the IncuCyte live-cell imaging platform. Cell growth was quantified based on the confluence area identified by the software-generated segmentation mask. Line plots show the temporal growth kinetics, and bar plots represent the corresponding area under the curve (AUC). DMSO (0.1%) served as the vehicle control. Data are presented as mean ± SD of independent experiments.

Figure 2. Transcriptomic changes induced by tacabrutideg and zanubrutinib in Karpas1718 marginal zone lymphoma cells.
(A-B) Volcano plots showing differentially expressed genes following exposure of Karpas1718 cells to tacabrutideg (5 nM; A) or zanubrutinib (5 nM; B) for 8, 12, and 24 hours, compared with DMSO-treated controls (0.1%). The x-axis represents the log2 fold-change and the y-axis the -log10 adjusted P-value. Significantly upregulated and downregulated genes are shown in red and blue, respectively, whereas non-significant genes are shown in gray. Selected differentially expressed genes are indicated.
(C) Gene Set Enrichment Analysis (GSEA) comparing tacabrutideg- and zanubrutinib-treated cells with DMSO controls. Bubble plots show significantly enriched gene sets following treatment with tacabrutideg (left) or zanubrutinib (right). Bubble size represents the number of genes contributing to each gene set, whereas color indicates the normalized enrichment score (NES). The plot shows significantly enriched gene sets ($P < 0.05$, adjusted $P < 0.25$, $|NES| > 1$).

Figure 3. **Tacabrutideg induces BTK degradation and suppresses downstream BCR signaling in Karpas1718 cells**.
Karpas1718 cells were treated with tacabrutideg or zanubrutinib at their respective IC_{50} $2\times IC_{50}$ and $5\times IC_{50}$ concentrations for 24 hours, with DMSO (0.1%) as vehicle control. Representative immunoblots showing phosphorylated and total BTK, PLCγ2, and ERK1/2 are presented. GAPDH was used as a loading control. Bar graphs show densitometric quantification of phosphorylated proteins normalized to their corresponding total protein (phospho/total ratio) and total protein abundance normalized to GAPDH. Protein levels are expressed relative to DMSO-treated cells. Data are presented as mean ± SD of at least 2 independent experiments. Statistical significance was determined by one-way ANOVA followed by Dunnett's multiple-comparison test, compared to the control (DMSO, grey bar). * $P < 0.05$; ** $P < 0.01$; *** $P < 0.001$.

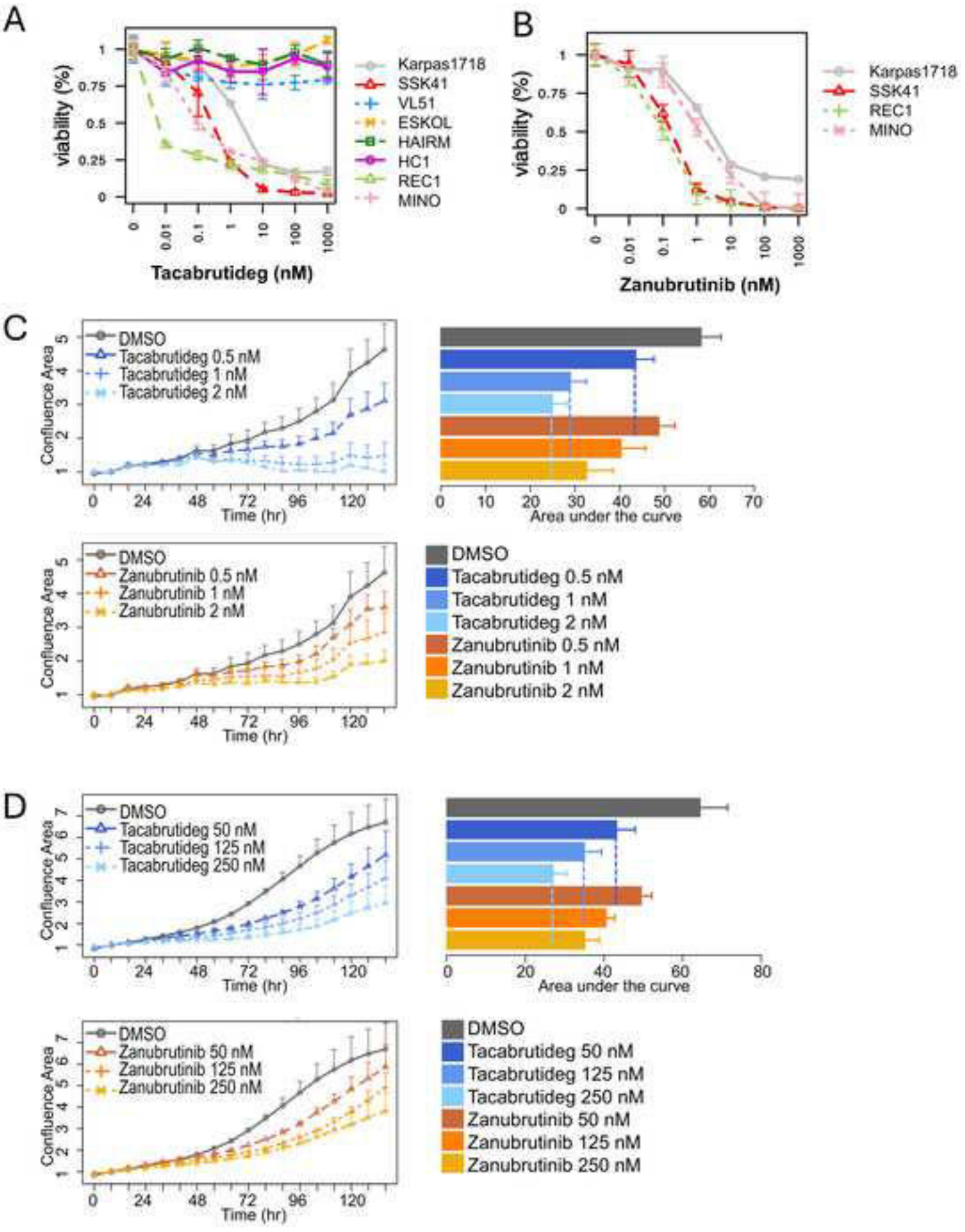
Figure 4. Antitumor activity of the combination of tacabrutideg and the BCL2 inhibitor sonrotoclax in marginal zone lymphoma models.
(A) Karpas1718, HC1, SSK41, and VL51 cells were exposed to increasing concentrations of tacabrutideg and sonrotoclax, either as single agents or in combination, for 5 days, followed by assessment of cell viability by MTT assay. Drug interaction matrices showing the effects of the combination of tacabrutideg and sonrotoclax in the four MZL cell lines. Drug interactions were evaluated using the Highest Single Agent (HSA) reference model implemented in the SynergyFinder platform. Red indicates synergistic interactions, white additive effects, and green antagonistic interactions. The HSA synergy score for each cell line is indicated above the corresponding matrix.
(B) Long-term growth of Karpas1718 (top) and VL51 (bottom) cells following treatment with DMSO (0.1%), tacabrutideg, sonrotoclax, or their combination, as monitored by live-cell imaging using the IncuCyte system for 6 days. Line graphs show changes in cell confluence over time.
(C) Representative immunoblots and densitometric quantification of BTK, phosphorylated BTK (pBTK), BCL2, BCL-xL, MCL1, phosphorylated PLCγ2 (pPLCγ2), and phosphorylated ERK1/2 (pERK1/2) in Karpas1718 cells following 24-hour treatment with tacabrutideg and/or sonrotoclax. Protein abundance was normalized to vinculin and expressed relative to DMSO-treated cells. Representative immunoblots from two independent experiments are shown. Data are presented as mean ± SD of independent experiments. Statistical significance was determined by one-way ANOVA followed by Dunnett's multiple-comparison test, comparing each treatment with the DMSO control. * $P < 0.05$; ** $P < 0.01$; *** $P < 0.001$.

Figure 5. Tacabrutideg and sonrotoclax retain activity in a three-dimensional stromal co-culture model.
VL51, Karpas1718, and SSK41 cells stably expressing mCherry were co-cultured with human bone marrow stromal cells and exposed to DMSO (0.1%), zanubrutinib (ZANU), tacabrutideg (TACAB), Sonrotoclax (SONRO), or the combination of tacabrutideg and sonrotoclax for 7 days.
(A) Representative fluorescence images acquired at day 7 following treatment. Images show viable fluorescent tumor cells under the indicated treatment conditions. Scale bars, 200 µm.
(B) Quantification of cell growth over time. Fluorescence intensity was measured on days 3, 5, and 7 and normalized to the corresponding day 1 value. Line graphs show the mean normalized fluorescence intensity ± SD for VL51 (top), Karpas1718 (middle), and SSK41 (bottom) cells. Growth curves were generated from the mean ± SD of at least four biological replicates.
(C) Heatmaps summarizing the normalized drug effect at day 5 and day 7 for each cell line. Fluorescence intensity was normalized to DMSO-treated controls, and color intensity represents the percentage of drug effect, with red indicating reduced treatment effect and blue indicating increased treatment effect. Statistical significance was determined by one-way ANOVA followed by Dunnett's multiple-comparison test, comparing each treatment with the DMSO control. * $P < 0.05$; ** $P < 0.01$; *** $P < 0.001$; **** $P < 0.0001$.

Figure 6. Tacabrutideg inhibits the growth of primary marginal zone lymphoma cells and modulates ERK signaling.
Results obtained from three primary marginal zone lymphoma samples: a primary splenic marginal zone lymphoma sample (Sample 1, A), and two nodal marginal zone lymphoma samples (Sample 2, B; Sample 3, C). Primary MZL cells were cultured *ex vivo* and treated with DMSO (0.1%), tacabrutideg (Tacab.,125 or 250 nM). Representative IncuCyte images acquired at baseline (0 hours) and after 72 hours of treatment are shown (top). Cell growth was continuously monitored by live-cell imaging for 72 hours, and the corresponding growth curves (center) are shown. Intracellular phosphorylated ERK1/2 (pERK, Thr202/Tyr204) was evaluated by flow cytometry in CD20-positive lymphoma cells after 24 hours of treatment (bottom left). Surface CD20 expression was confirmed by flow cytometry in lymphoma at baseline (0 hours, bottom right).

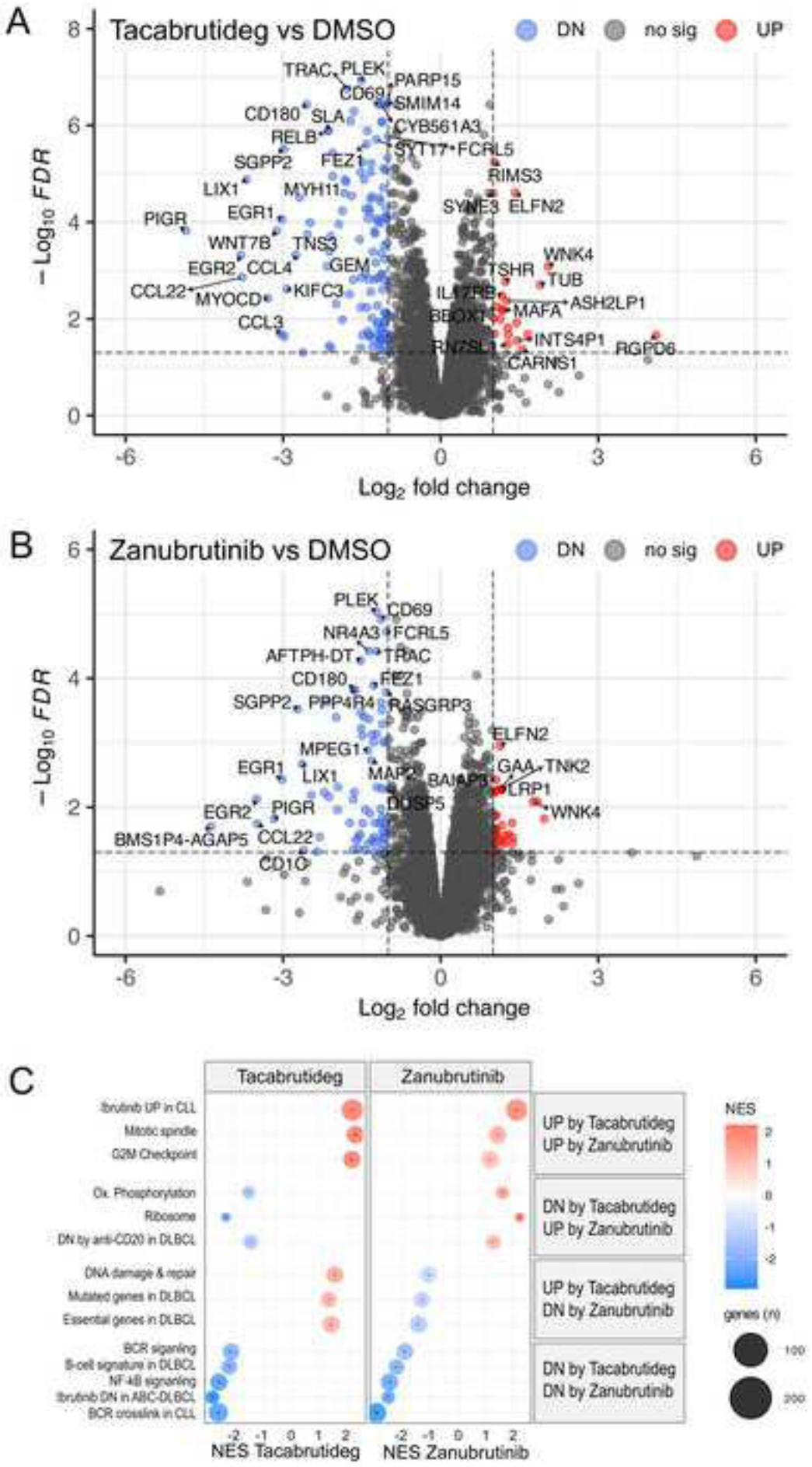
Figure

Click here to access/download;Figure;Figure 1.jpg



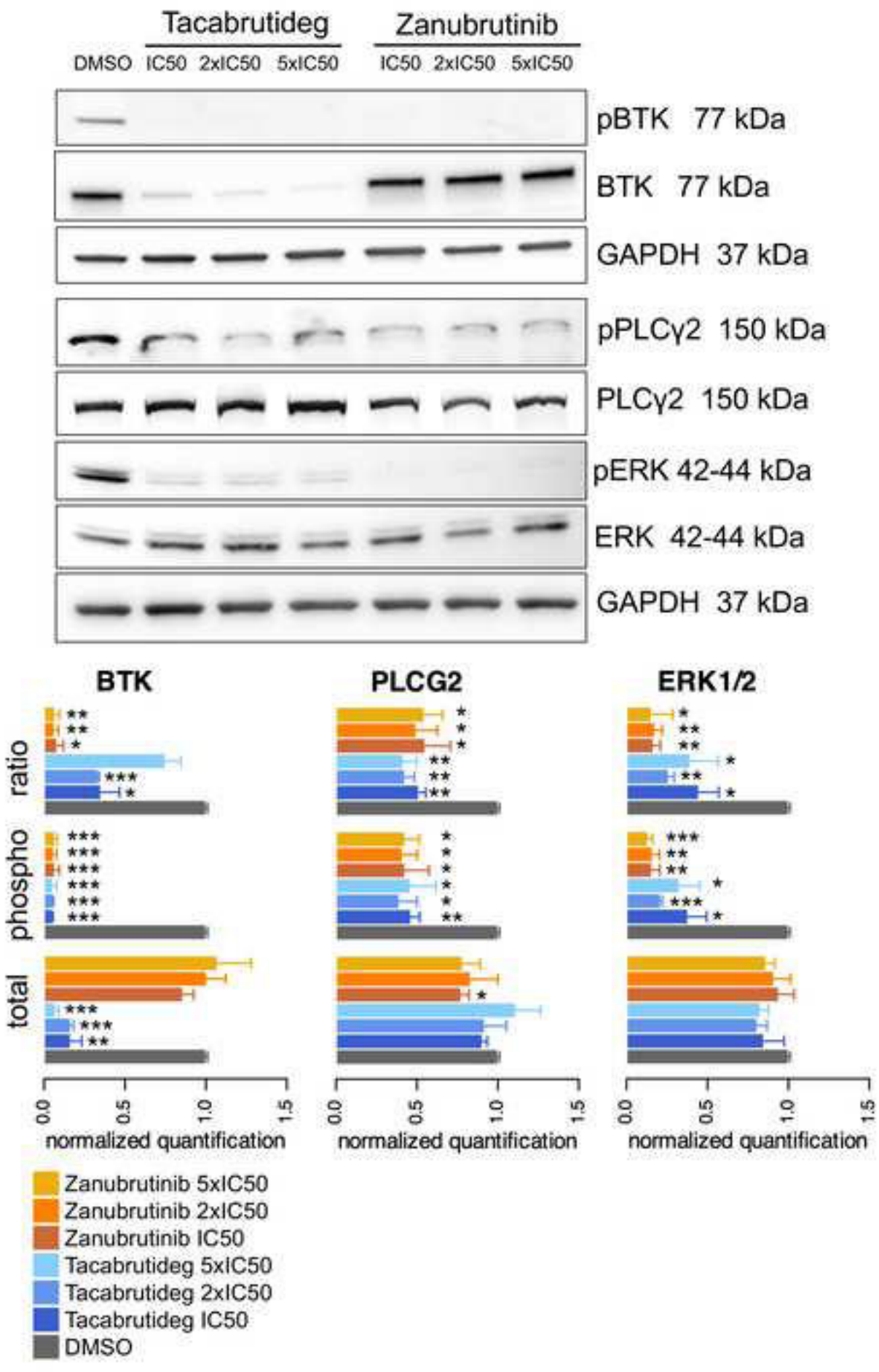
Figure

Click here to access/download;Figure;Figure 2_new.jpg



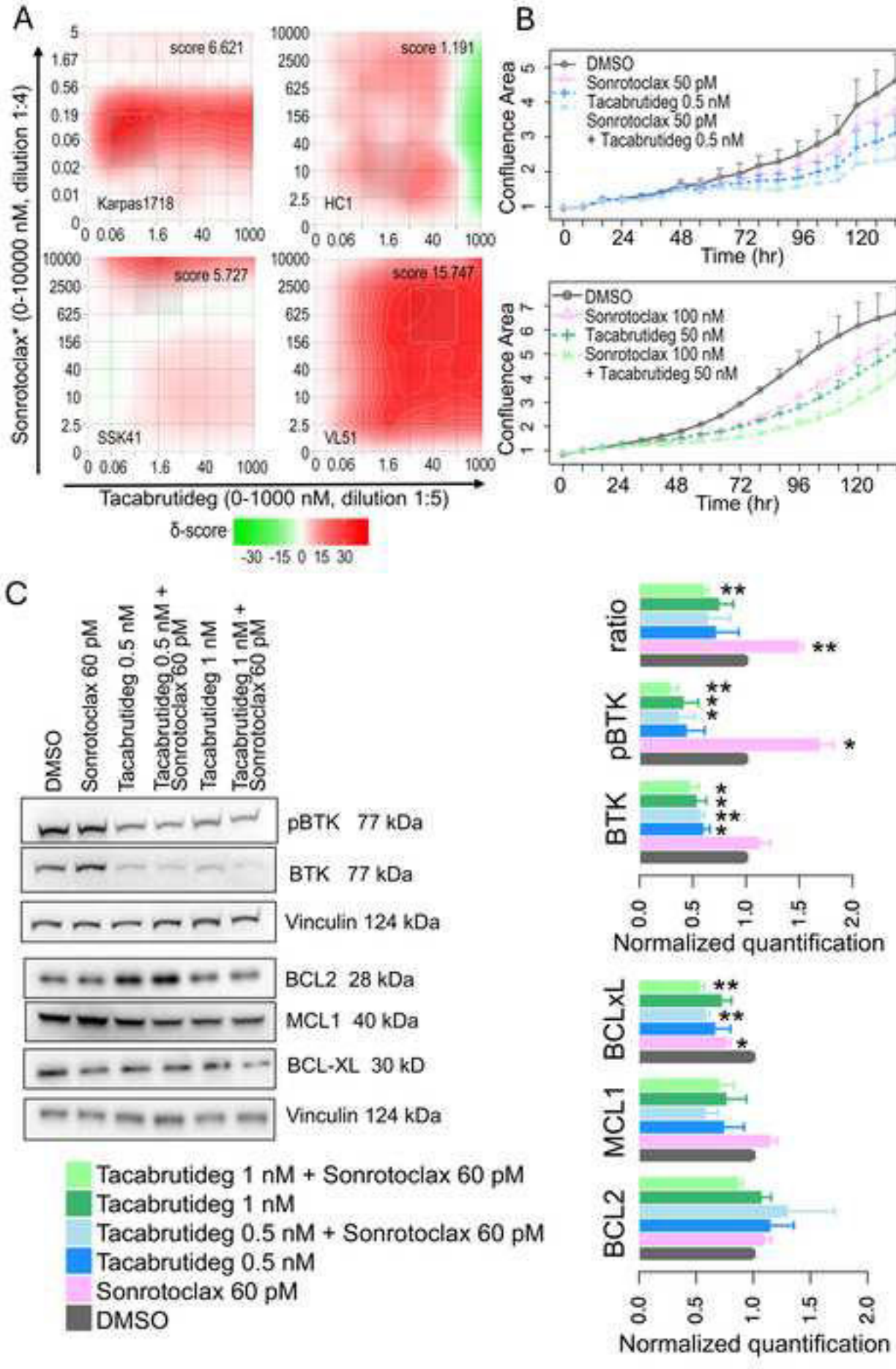
Figure

Click here to access/download;Figure;Figure 3_new.jpg



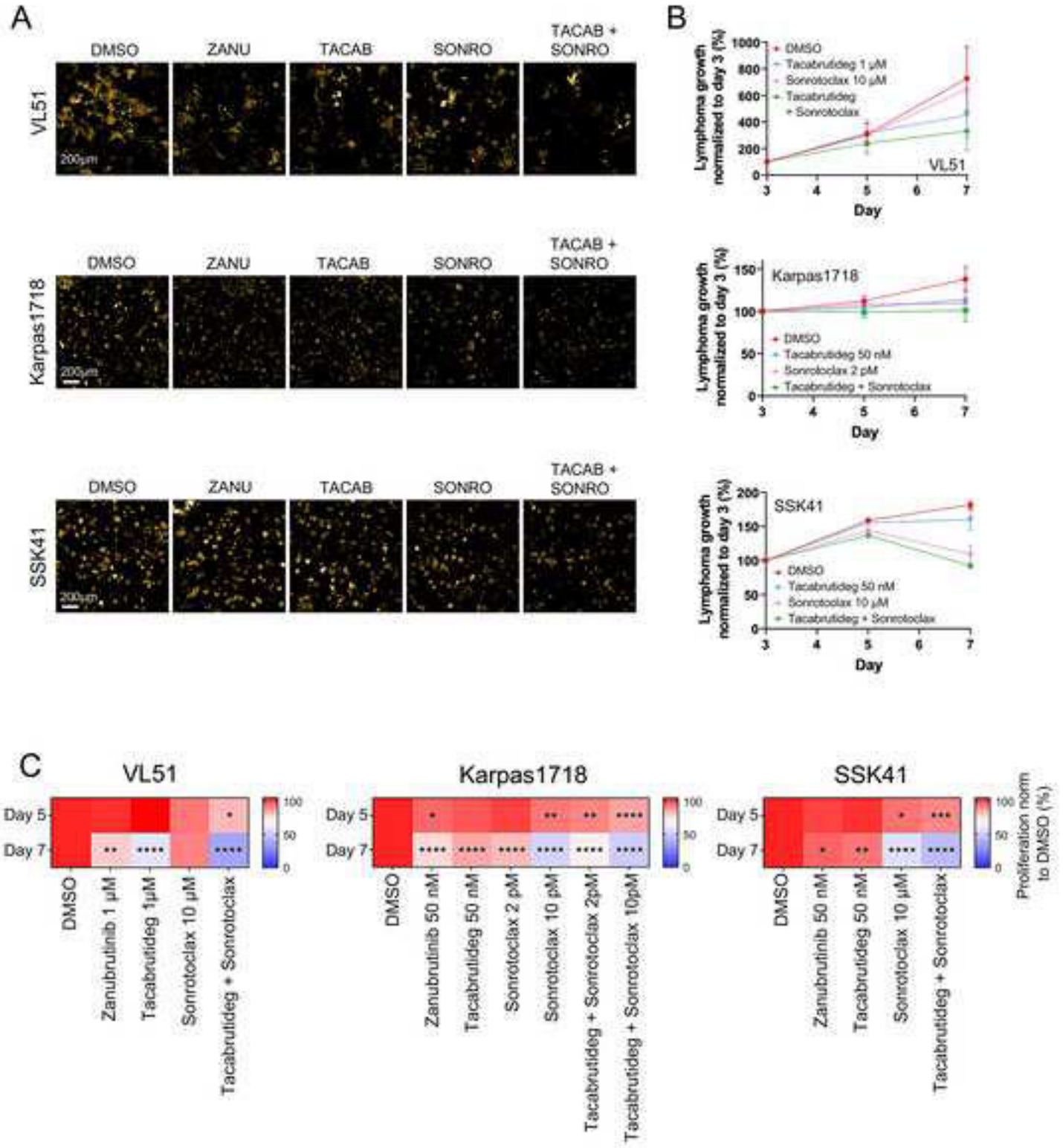
Figure

Click here to access/download;Figure;Figure 4_new_v2.jpg



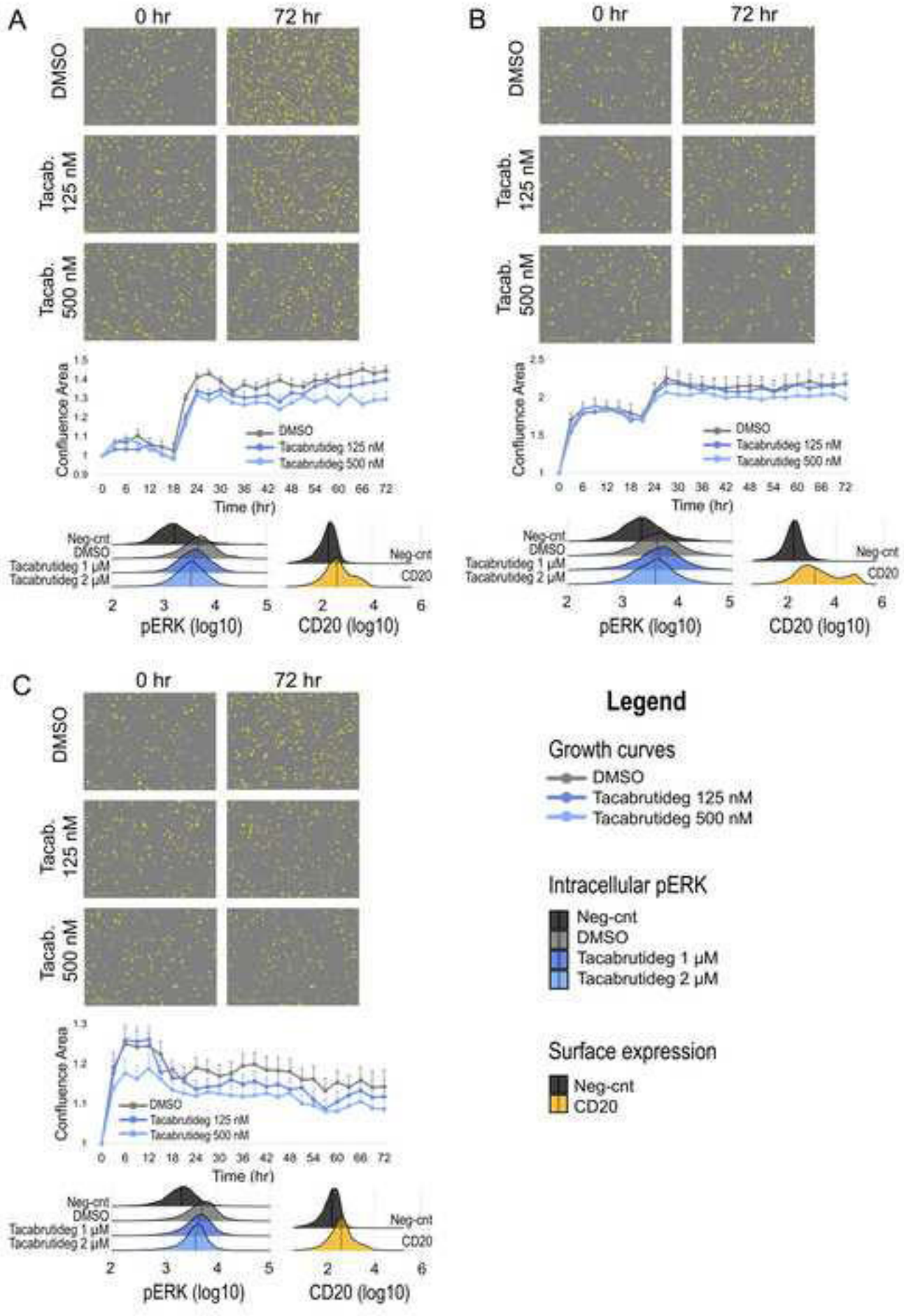
Figure

Click here to access/download;Figure;Figure 5 v4.jpg



Figure

Click here to access/download;Figure;Figure 6.jpg



Dual targeting of BTK and BCL2 enhances apoptosis in marginal zone lymphoma: preclinical activity of BGB-16673 and Sonrotoclax

Supplementary methods

Primary marginal zone lymphoma (MZL) samples

Fresh lymph nodes or spleen were processed under sterile conditions in a biological safety cabinet. Primary samples (n=3; one splenic MZL and two nodal MZL) were mechanically dissociated using sterile scalpels in Petri dishes kept on ice to obtain a cell suspension. The resulting suspension was diluted with 0.9% NaCl and centrifuged. Following centrifugation, the supernatant was discarded, and the cell pellet was retained for cryopreservation. For cell freezing, two cryoprotective solutions were prepared: Solution A consisting of 40% RPMI-1640 medium and 60% fetal bovine serum (FBS), and Solution B consisting of 80% RPMI-1640 medium and 20% dimethyl sulfoxide (DMSO). The cell pellet was gently resuspended in an equal mixture of Solutions A and B. The resulting cell suspension was aliquoted into cryovials, containing approximately 30 million cells per vial. The cryovials were initially stored at −80°C in isopropanol freezing containers and subsequently transferred to liquid nitrogen for long-term preservation.

Primary cells were exposed to tacabrutideg (BGB-16673) at the indicated concentrations. Surface CD20 expression (PE, B&D Bioscience) was analyzed by flow cytometry. Cell growth was monitored for 72 hours using IncuCyte live-cell imaging and quantified as confluence area and area under the curve. In parallel, cells were exposed to Tacabrutideg for 24 hours and analyzed by flow cytometry for intracellular phospho-ERK (Thr202/Tyr204, Alexa Fluor 488, B&D Biosciences). The study was conducted in accordance with the ethical rules and regulatory requirements of the country in which it was performed.

Primary cells for 3D model

The human-derived specimen sampling was conducted under the guidelines, regulations, and procedures of the Ente Ospedaliero Cantonale (Bellinzona, Switzerland) and approved by the local IRB (Approval n. 2020-00029 from Comitato Etico Cantonale). The biological samples used in the study are represented by waste surgical pieces, harvested from patients who signed an informed consent. All the individuals were subjected to knee replacement surgery and presented OA Kellgren Lawrence grade 3 to 4, evaluated from radiological images. The patients' ages ranged from 58 to 73 years.

Isolation of primary Bone Marrow Stromal Cells (BMSCs) and culture conditions

Primary BMSCs were isolated from knee biopsies, as previously reported (1). After isolation, BMSCs were cryopreserved at -150°C, and all experiments were conducted within three weeks of thawing. To create pooled BMSCs, equal numbers of cells from each donor were combined. The pooled cells were then plated and cultured until passage 3, at which point they were used for experiments.

BMSCs were cultured in MEM Alpha medium (12571063, Gibco) supplemented with 10% fetal bovine serum (FBS; F9665, Sigma-Aldrich), 1% HEPES (15630056, Gibco), 1% Penicillin-Streptomycin (P/S, 10,000 U/mL; 15140122, Gibco), and 5 ng/mL basic fibroblast growth factor (100-18B, Peprotech).

Seeding in 3D fibrin gel

Cell-laden fibrin gels were prepared by suspending lymphoma cells and BMSCs in 4 U/mL thrombin (obtained from the TISSEEL Fibrin Sealant Kit, 025243179, Baxter), diluted in RPMI1640 supplemented with L-glutamine, 10% FBS, and 1% P/S. The solution was then mixed with an equal volume of 10 mg/mL fibrinogen (F3879, Sigma) to achieve a final fibrin concentration of 5 mg/mL. After combining fibrinogen and thrombin, the gels were allowed to polymerize at 37°C for 20 minutes. To maintain sterile conditions, automated high-throughput seeding was performed using the OT-2 liquid handler (Opentrons) equipped with a HEPA module. Cells were seeded into 50 µL fibrin gels in Nunc MicroWell 96-Well plates (167008, Thermo Scientific).

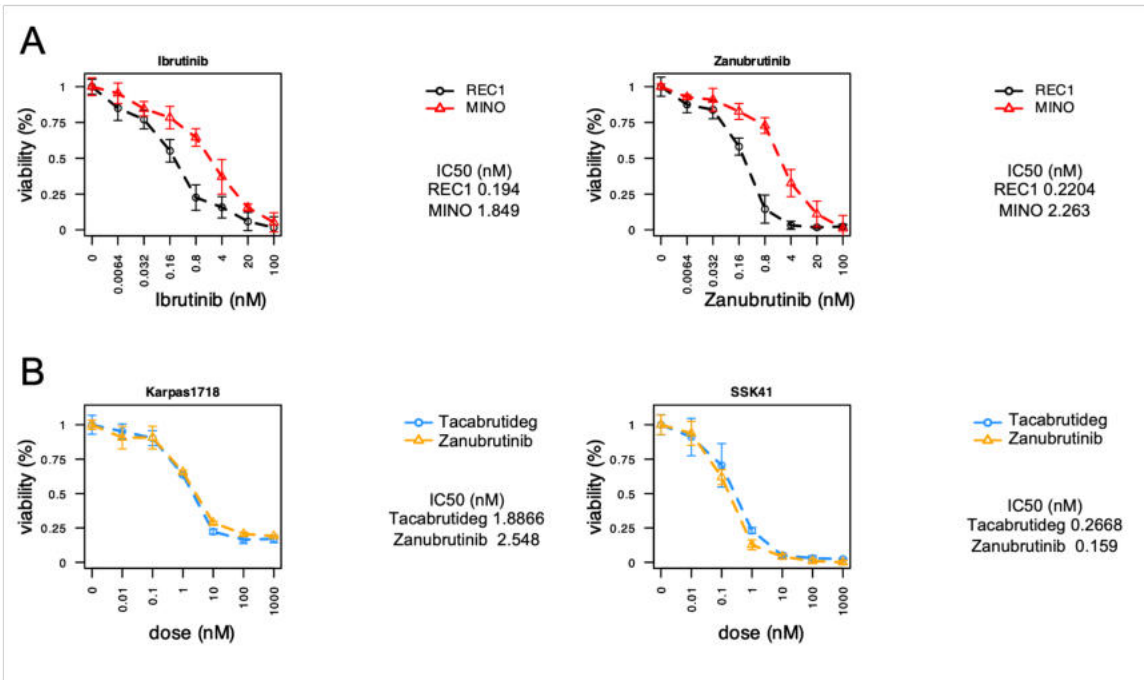
Treatment and cell proliferation evaluation in 3D fibrin gel

The mCherry-VL51 cells were seeded at 0.2 x 10^6 cells/mL; the mCherry-K1718 cells at 1 x 10^6 cells/mL; and the mCherry-SSK41 cells at 0.5 x 10^6 cells/mL. All models were co-cultured with primary BMSCs seeded at 0.75 x 10^6 cells/mL. Cells were maintained in RPMI-1640 supplemented with L-glutamine, 10% FBS, and 1% P/S. On day 3, specific treatment conditions, as indicated in the respective figures, were initiated. On day 5, fresh treatment-conditioned medium was added. Live imaging of the cultures was performed on days 3, 5, and 7 using the Opera Phenix Plus High-Content Screening System (PerkinElmer) while maintaining the plate at 37°C, 5% CO_2, and optimal humidity. Treatment effects were assessed by both morphological observations and quantitative image analysis. The growth curve for each condition was generated by measuring the total mCherry$^+$ area from the maximum-projection images, first normalizing to the respective well at day 3 (normalized proliferation value), then to the DMSO control for each condition (drug effect, expressed as a percentage).

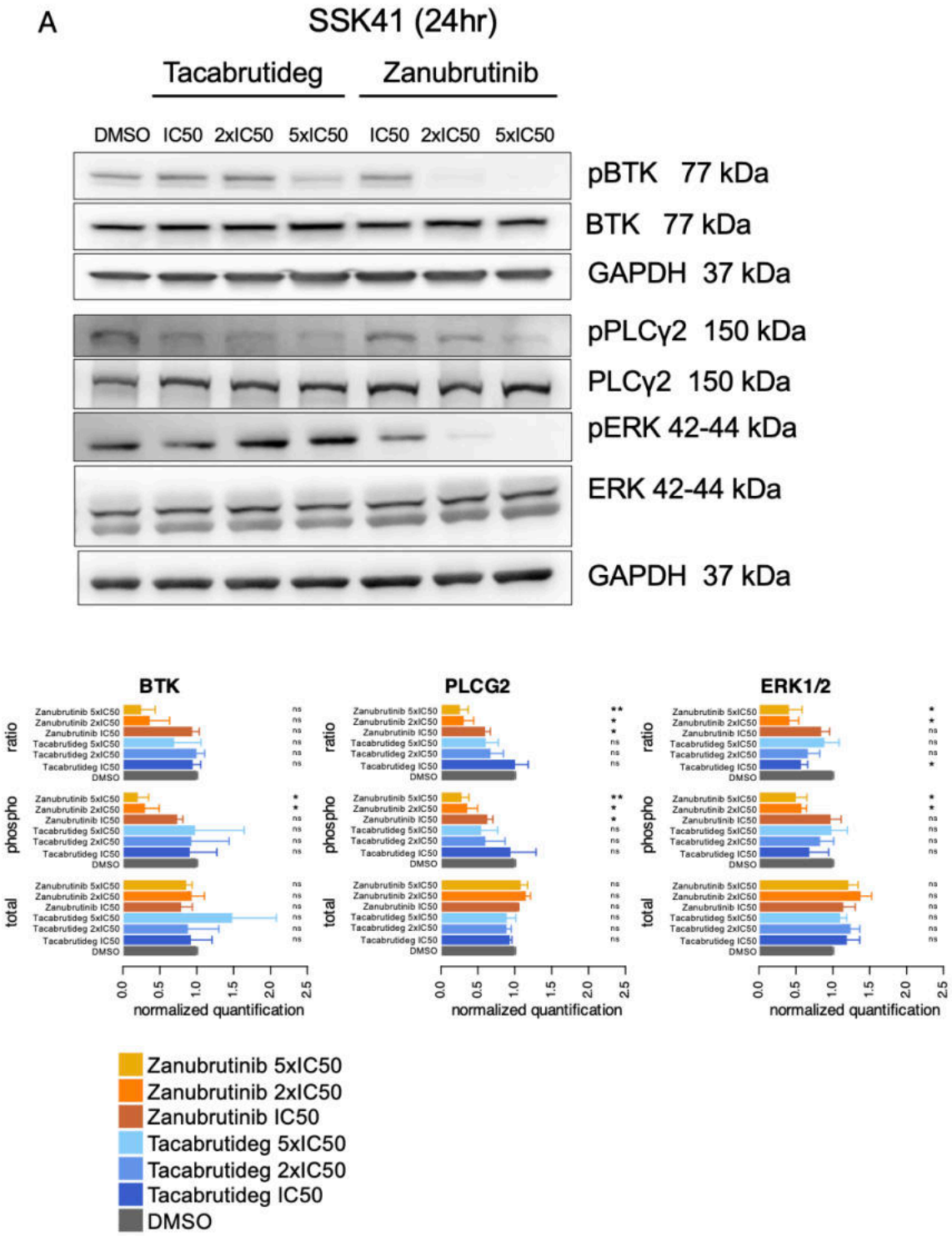
1. D. Petta, D. D'Arrigo, S. Salehi, et al. A personalized osteoarthritic joint-on-a-chip as a screening platform for biological treatments. *Materials Today. Bio*. 2024; 26: 101072.

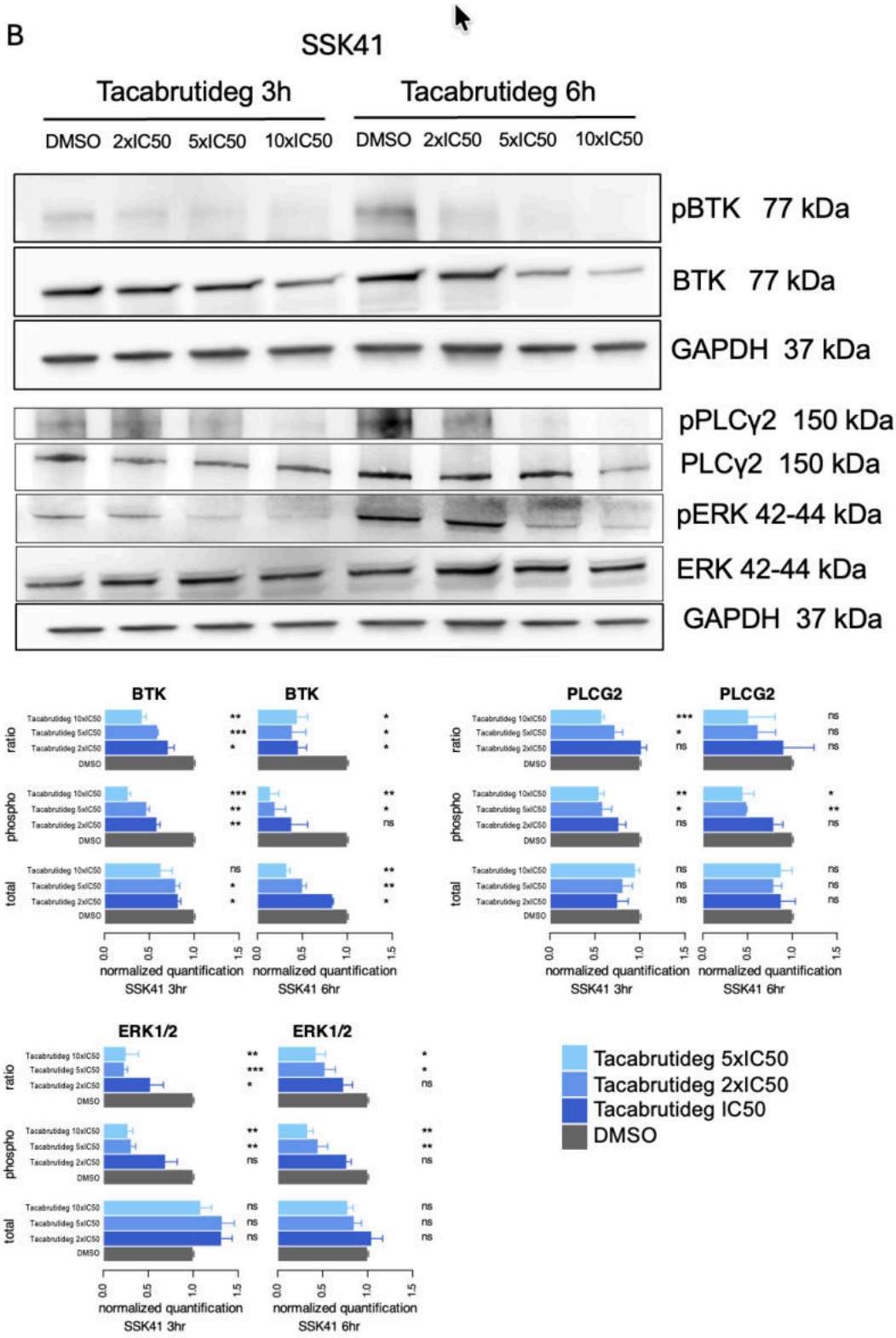
Supplementary figures and tables

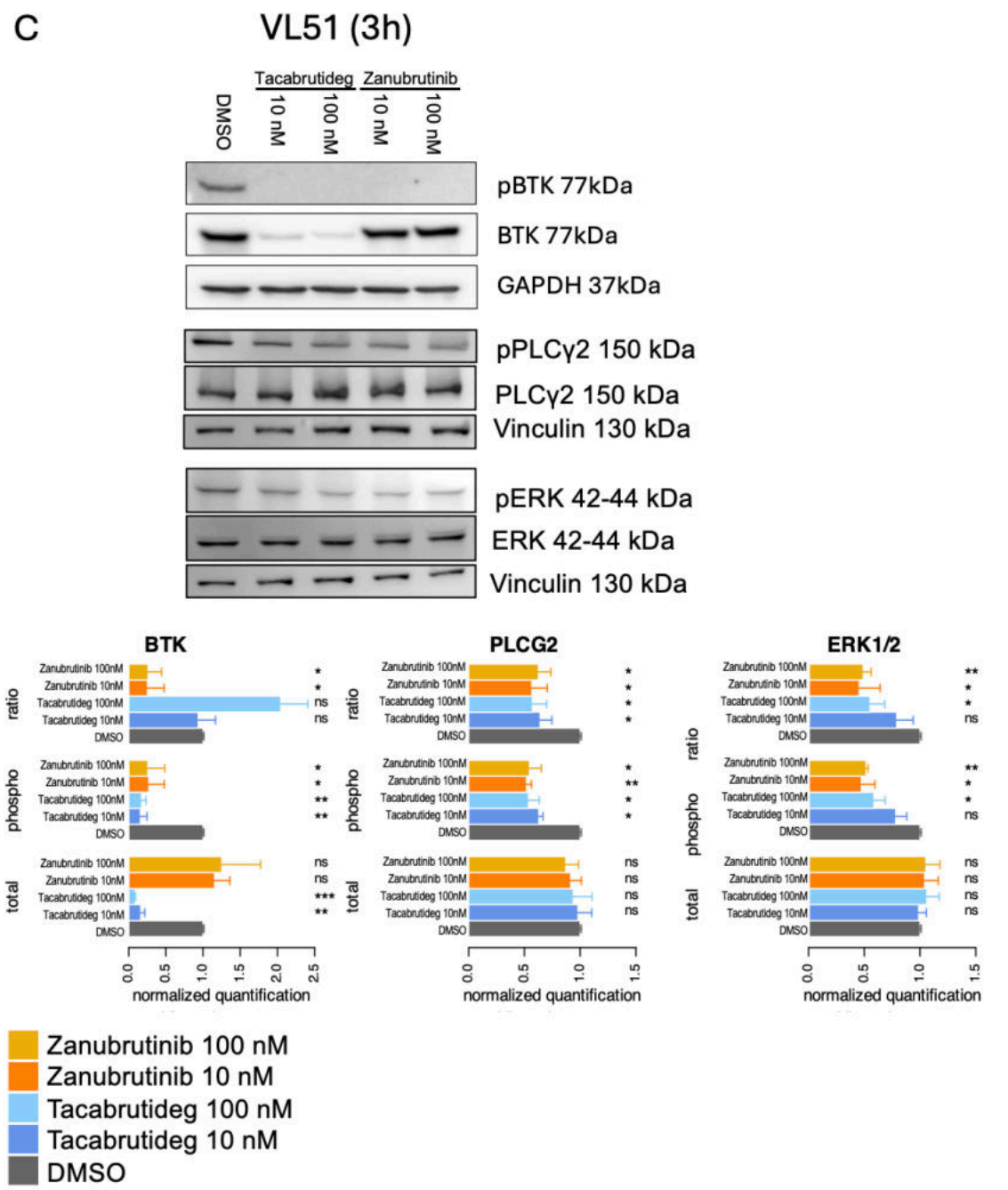
Supplementary Figure 1. Effect of exposure to the BTK inhibitors ibrutinib and zanubrutinib, or the BTK-degrader BGB-16673 in MCL and MZL cell lines. (A) Effect of exposure to the BTK inhibitors ibrutinib or zanubrutinib in two MCL cell lines, REC1 (black) and MINO (red). (B) Effect of exposure to the BTK-degrader tacabrutideg (blue) or to the BTK inhibitor zanubrutinib (orange) in two MZL cell lines, Karpas1718 (left) and SSK41 (right). MTT assay after five days of exposure.



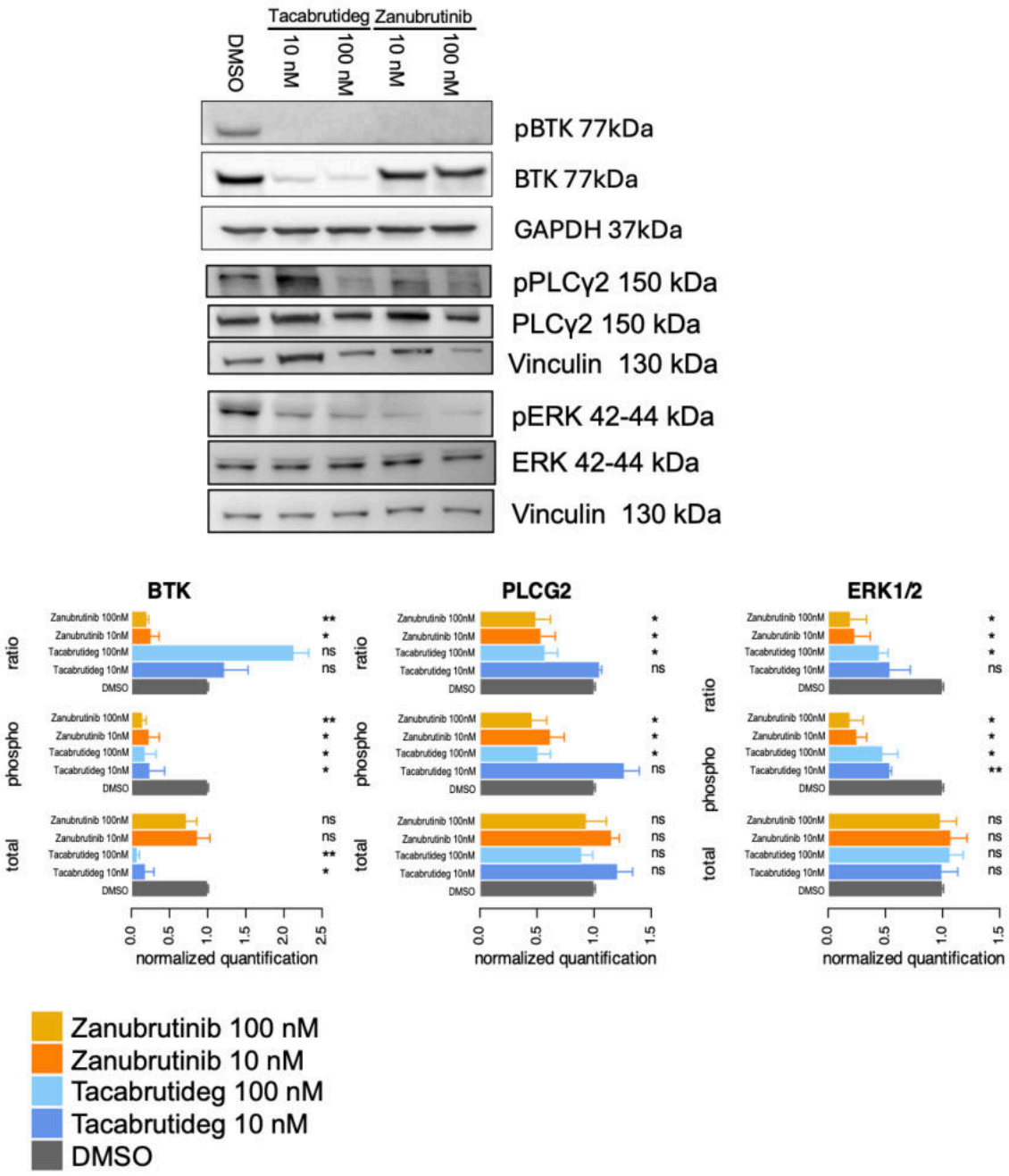
Supplementary Figure 2. Effect of the BTK-degrader tacabrutideg and the BTK inhibitor zanubrutinib on the protein levels of total, phosphorylated, and the phosphorylated/total ratio of BTK, PLCG2, and ERK1/2 in the MZL cell lines SSK41 (24hr, A; 3hr and 6hr, B), VL51 (3hr, C), ESKOL (3hr, D), HAIRM, (3hr, E), and HC1 (3hr, F). Immunoblotting is representative of two independent experiments. Each barplot shows the mean protein quantification in the two experiments; error bars correspond to the standard deviation of the mean. Statistical significance was determined by one-way ANOVA followed by Dunnett's multiple-comparison test, compared to the control (DMSO, grey bar). * $P < 0.05$; ** $P < 0.01$; *** $P < 0.001$; ns, not significant. (G) Protein levels of total, phosphorylated, and the phosphorylated/total ratio of BTK (top and left middle panels, blue) upon Tacabrutideg (BGB-16673), and IC50 values (right panel, red), were compared between sensitive (Karpas1718 and SSK41) and primary resistant (VL51, ESKOL, HAIRM, and HC1) cell lines by *t-test*. The bottom panel shows a heatmap of the protein levels of BTK, pBTK, and pBTK/BTK across cell lines tested.


A
SSK41 (24hr)
Tacabrutideg
Zanubrutinib
DMSO IC50 2xIC50 5xIC50 IC50 2xIC50 5xIC50
pBTK 77 kDa
BTK 77 kDa
GAPDH 37 kDa
pPLCγ2 150 kDa
PLCγ2 150 kDa
pERK 42-44 kDa
ERK 42-44 kDa
GAPDH 37 kDa
BTK
PLCG2
ERK1/2
ratio
phospho
total
normalized quantification
Zanubrutinib 5xIC50
Zanubrutinib 2xIC50
Zanubrutinib IC50
Tacabrutideg 5xIC50
Tacabrutideg 2xIC50
Tacabrutideg IC50
DMSO

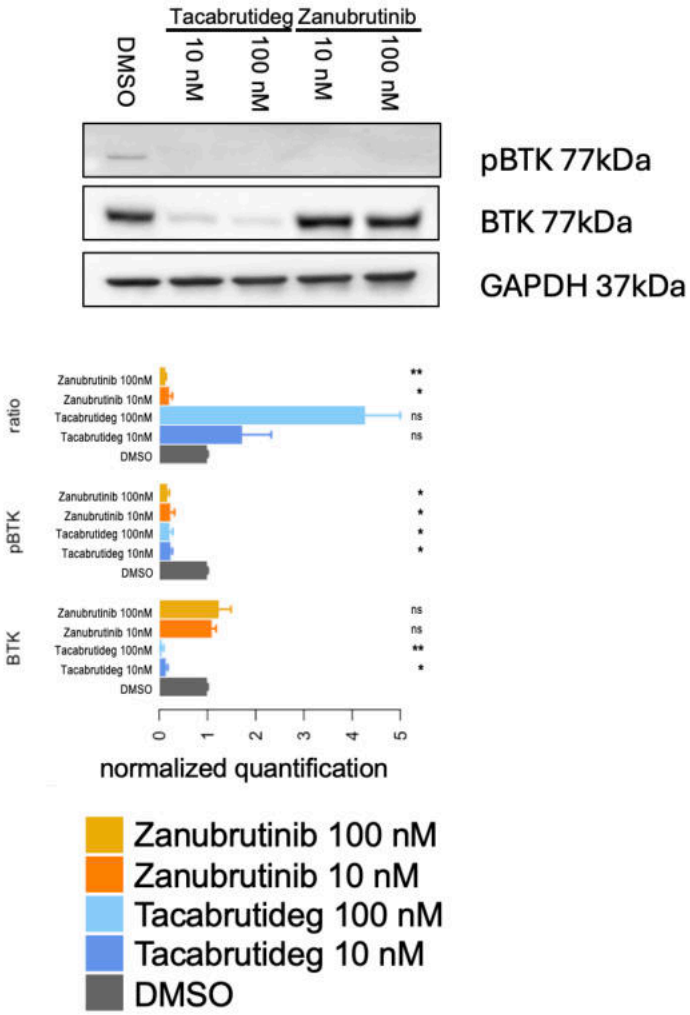

B
SSK41
Tacabrutideg 3h
Tacabrutideg 6h
DMSO 2xIC50 5xIC50 10xIC50
DMSO 2xIC50 5xIC50 10xIC50
pBTK 77 kDa
BTK 77 kDa
GAPDH 37 kDa
pPLCγ2 150 kDa
PLCγ2 150 kDa
pERK 42-44 kDa
ERK 42-44 kDa
GAPDH 37 kDa
BTK
BTK
PLCG2
PLCG2
ERK1/2
ERK1/2
ratio
phospho
total
Tacabrutideg 10xIC50
Tacabrutideg 5xIC50
Tacabrutideg 2xIC50
DMSO
normalized quantification
SSK41 3hr
SSK41 6hr
Tacabrutideg 5xIC50
Tacabrutideg 2xIC50
Tacabrutideg IC50
DMSO


C
VL51 (3h)
Tacabrutideg
Zanubrutinib
DMSO
10 nM
100 nM
10 nM
100 nM
pBTK 77kDa
BTK 77kDa
GAPDH 37kDa
pPLCγ2 150 kDa
PLCγ2 150 kDa
Vinculin 130 kDa
pERK 42-44 kDa
ERK 42-44 kDa
Vinculin 130 kDa
BTK
PLCG2
ERK1/2
ratio
phospho
total
Zanubrutinib 100nM
Zanubrutinib 10nM
Tacabrutideg 100nM
Tacabrutideg 10nM
DMSO
normalized quantification
Zanubrutinib 100 nM
Zanubrutinib 10 nM
Tacabrutideg 100 nM
Tacabrutideg 10 nM
DMSO

D

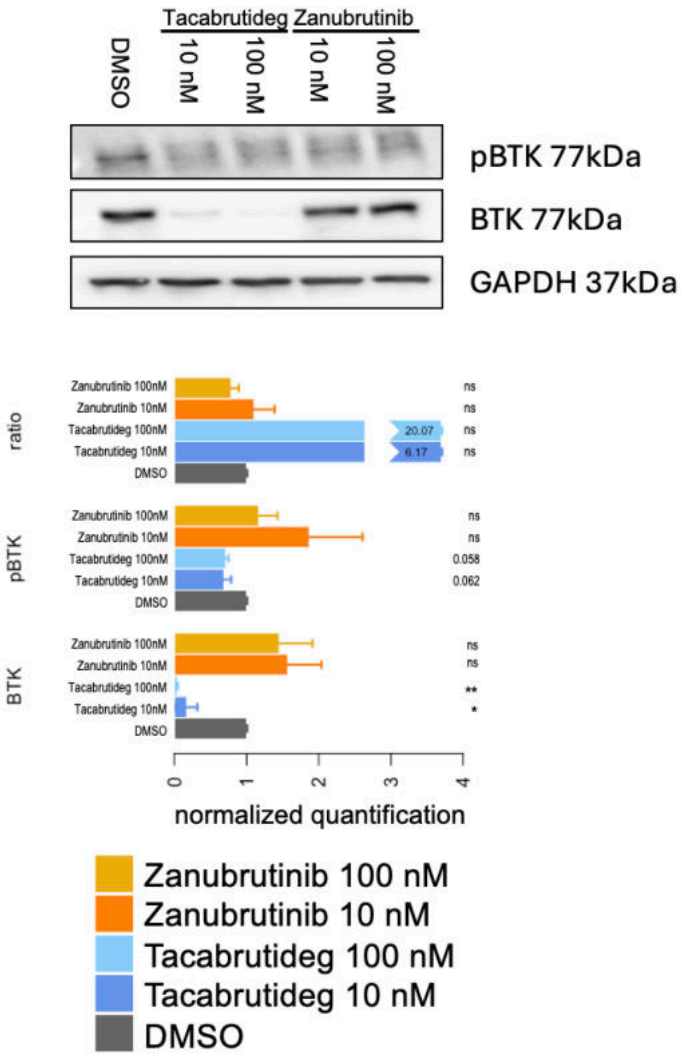

ESKOL 3hr
Tacabrutideg
Zanubrutinib
DMSO
10 nM
100 nM
10 nM
100 nM
pBTK 77kDa
BTK 77kDa
GAPDH 37kDa
pPLCγ2 150 kDa
PLCγ2 150 kDa
Vinculin 130 kDa
pERK 42-44 kDa
ERK 42-44 kDa
Vinculin 130 kDa
BTK
PLCG2
ERK1/2
ratio
phospho
total
Zanubrutinib 100nM
Zanubrutinib 10nM
Tacabrutideg 100nM
Tacabrutideg 10nM
DMSO
normalized quantification
Zanubrutinib 100 nM
Zanubrutinib 10 nM
Tacabrutideg 100 nM
Tacabrutideg 10 nM
DMSO

E HAIRM 3h

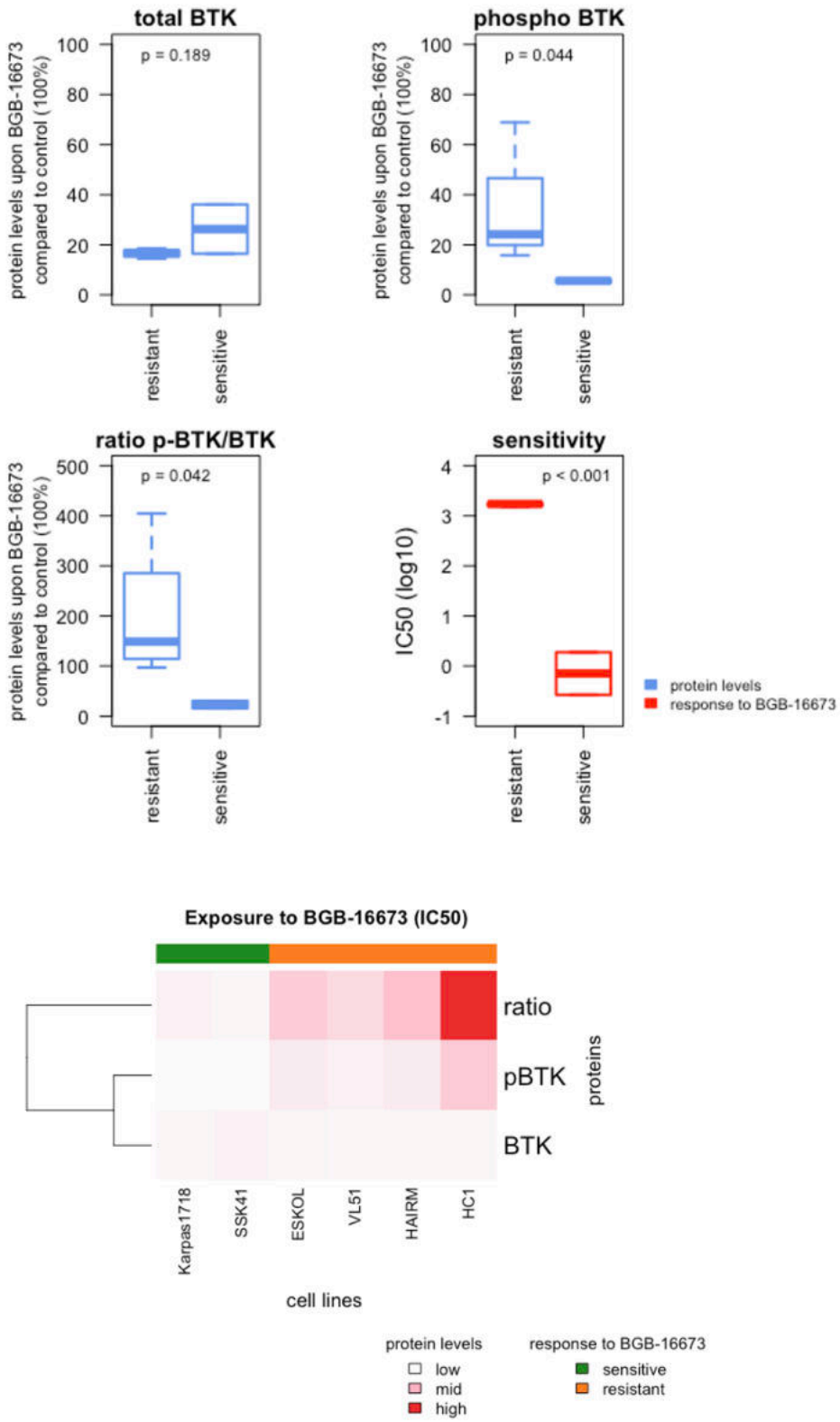

Tacabrutideg
Zanubrutinib
DMSO
10 nM
100 nM
10 nM
100 nM
pBTK 77kDa
BTK 77kDa
GAPDH 37kDa
ratio
pBTK
BTK
Zanubrutinib 100nM
Zanubrutinib 10nM
Tacabrutideg 100nM
Tacabrutideg 10nM
DMSO
**
*
ns
ns
*
*
*
*
ns
ns
**
*
0
1
2
3
4
5
normalized quantification
Zanubrutinib 100 nM
Zanubrutinib 10 nM
Tacabrutideg 100 nM
Tacabrutideg 10 nM
DMSO

F

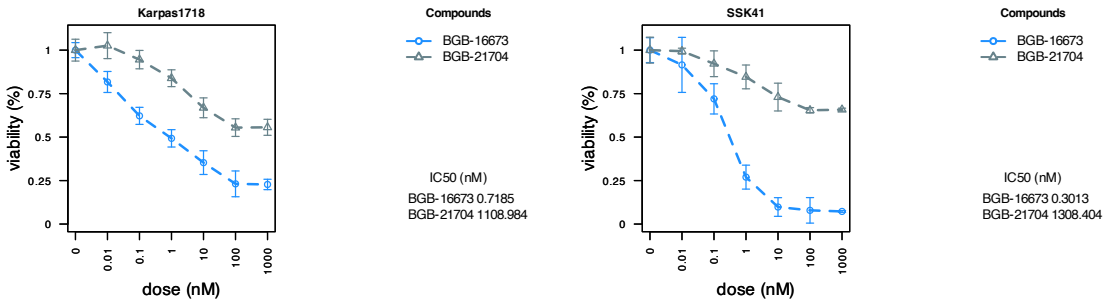
HC1


Tacabrutideg
Zanubrutinib
DMSO
10 nM
100 nM
10 nM
100 nM
pBTK 77kDa
BTK 77kDa
GAPDH 37kDa
ratio
pBTK
BTK
Zanubrutinib 100nM
Zanubrutinib 10nM
Tacabrutideg 100nM
Tacabrutideg 10nM
DMSO
20.07
6.17
ns
0.058
0.062
**
*
0
1
2
3
4
normalized quantification
Zanubrutinib 100 nM
Zanubrutinib 10 nM
Tacabrutideg 100 nM
Tacabrutideg 10 nM
DMSO

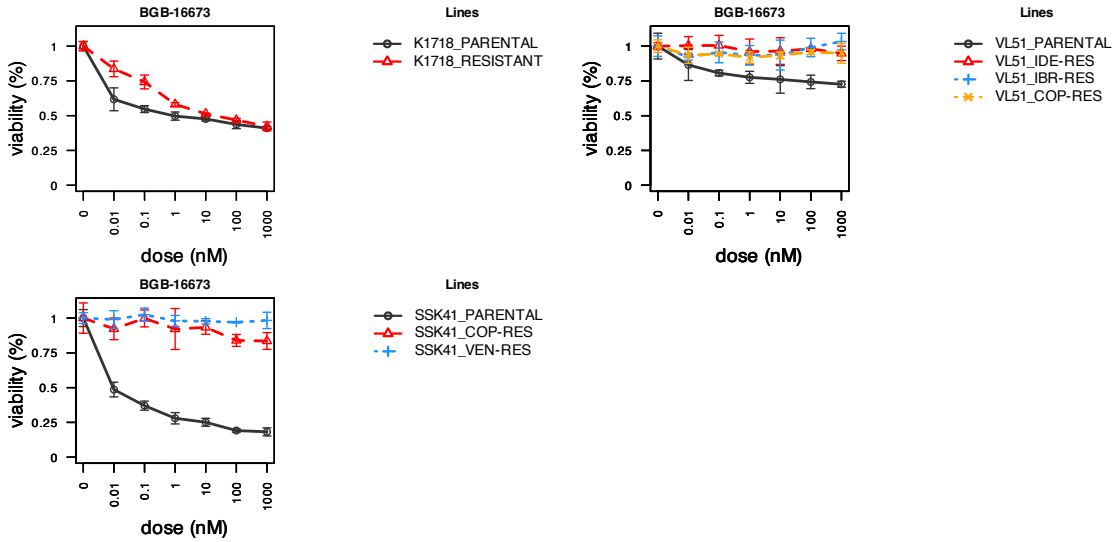
G


total BTK
p = 0.189
protein levels upon BGB-16673 compared to control (100%)
resistant
sensitive
phospho BTK
p = 0.044
ratio p-BTK/BTK
p = 0.042
sensitivity
p < 0.001
IC50 (log10)
protein levels
response to BGB-16673
Exposure to BGB-16673 (IC50)
ratio
pBTK
BTK
proteins
Karpas1718
SSK41
ESKOL
VL51
HAIRM
HC1
cell lines
protein levels
low
mid
high
response to BGB-16673
sensitive
resistant

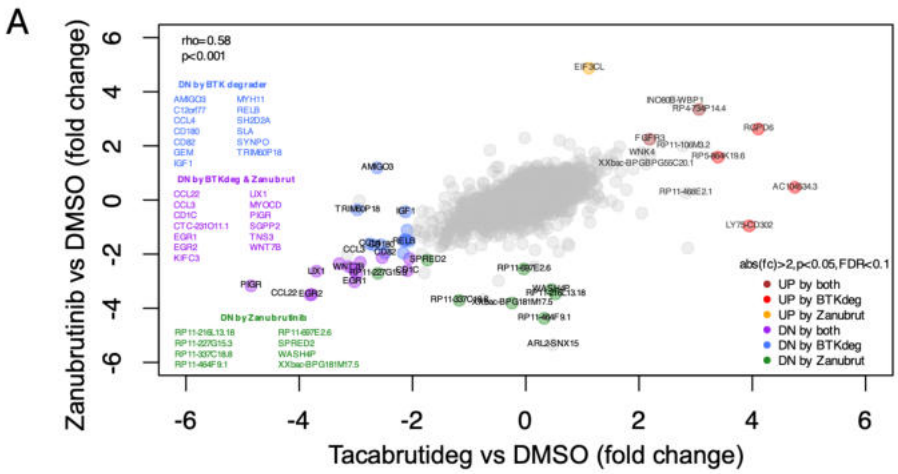
Supplementary Figure 3. Effect of five days of exposure to the BTK-degrader tacabrutideg (BGB-16673) and of BGB-21704, a similar drug to BGB-16673 with no BTK-related activity, in the two MZL cell lines Karpas1718 (left panel) and SSK41 (right panel). MTT after 5 days of exposure. Blue, BGB-16673. grey, BGB-21704.

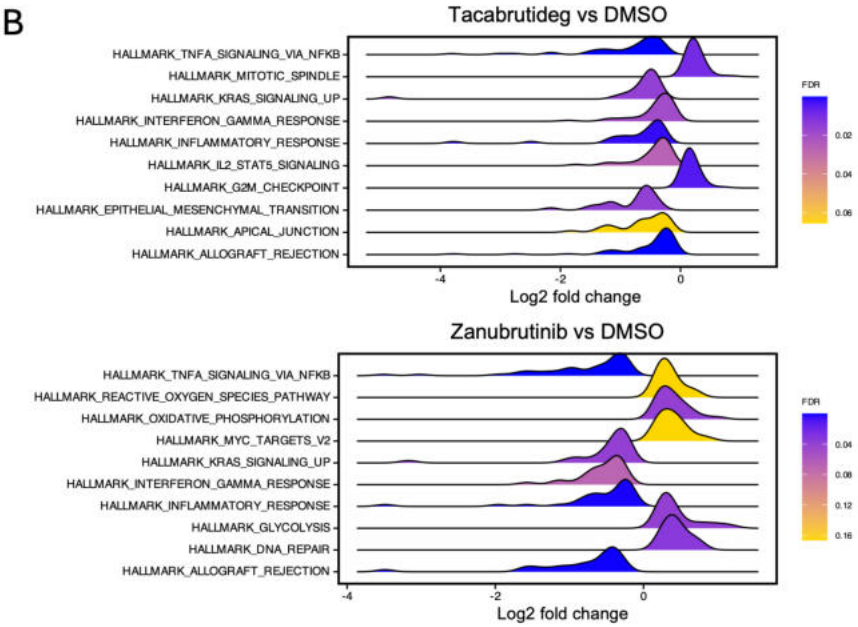


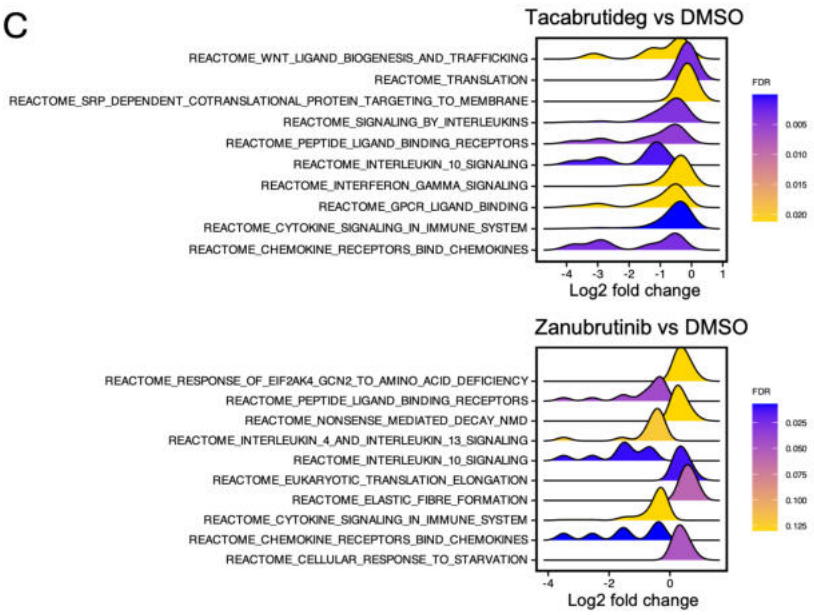
Supplementary Figure 4. Effect of five days of exposure to the BTK-degrader tacabrutideg (BGB-16673) in parental and resistant derivatives to PI3K, BTK, and BCL2 inhibitors, derived from Karpas1718 (top left), VL51 (top right), and SSK41 (bottom left). MTT after 5 days of exposure.



Supplementary Figure 5. Functional enrichment analyses from gene expression profiles of tacabrutideg or zanubrutinib when compared to DMSO. (A) Correlation plot of the fold-change of transcripts after tacabrutideg (BGB-16673, X-axis) or zanubrutinib (Y-axis) versus DMSO. Ridgeline plots of the distribution of the core-enriched genes of the top 10 significantly deregulated genesets from MSigDB Hallmarks (B) and Reactome (C) pathways of tacabrutideg (BGB-16673, top) or zanubrutinib (bottom) expression profiles. (D) Heatmaps showing gene-level expression changes within representative GSEA-enriched pathways following treatment with tacabrutideg (green) or zanubrutinib (yellow). Each row represents one gene belonging to the indicated signature, and colors indicate normalized expression changes relative to DMSO. Hierarchical clustering highlights the similarities and differences between the transcriptional programs regulated by BTK degradation and BTK inhibition.


A
rho=0.58
p<0.001
DN by BTK degrader
AMIGO3
C12orf77
CCL4
CD180
CD82
GEM
IGF1
MYH11
RELB
SH2D2A
SLA
SYNPO
TRIM69P18
DN by BTKdeg & Zanubrut
CCL22
CCL3
CD1C
CTC-251O11.1
EGR1
EGR2
KIFC3
UX1
MYOCD
PIGR
SGPP2
TNS3
WNT7B
DN by Zanubrutinib
RP11-216L13.18
RP11-227G15.3
RP11-337C18.8
RP11-464F9.1
RP11-687E2.6
SPRED2
WASH4P
XXbac-BPG181M17.5
abs(fc)>2,p<0.05,FDR<0.1
UP by both
UP by BTKdeg
UP by Zanubrut
DN by both
DN by BTKdeg
DN by Zanubrut
Zanubrutinib vs DMSO (fold change)
Tacabrutideg vs DMSO (fold change)


B
Tacabrutideg vs DMSO
HALLMARK_TNFA_SIGNALING_VIA_NFKB
HALLMARK_MITOTIC_SPINDLE
HALLMARK_KRAS_SIGNALING_UP
HALLMARK_INTERFERON_GAMMA_RESPONSE
HALLMARK_INFLAMMATORY_RESPONSE
HALLMARK_IL2_STAT5_SIGNALING
HALLMARK_G2M_CHECKPOINT
HALLMARK_EPITHELIAL_MESENCHYMAL_TRANSITION
HALLMARK_APICAL_JUNCTION
HALLMARK_ALLOGRAFT_REJECTION
FDR
Log2 fold change
Zanubrutinib vs DMSO
HALLMARK_TNFA_SIGNALING_VIA_NFKB
HALLMARK_REACTIVE_OXYGEN_SPECIES_PATHWAY
HALLMARK_OXIDATIVE_PHOSPHORYLATION
HALLMARK_MYC_TARGETS_V2
HALLMARK_KRAS_SIGNALING_UP
HALLMARK_INTERFERON_GAMMA_RESPONSE
HALLMARK_INFLAMMATORY_RESPONSE
HALLMARK_GLYCOLYSIS
HALLMARK_DNA_REPAIR
HALLMARK_ALLOGRAFT_REJECTION
FDR
Log2 fold change


C
Tacabrutideg vs DMSO
REACTOME_WNT_LIGAND_BIOGENESIS_AND_TRAFFICKING
REACTOME_TRANSLATION
REACTOME_SRP_DEPENDENT_COTRANSLATIONAL_PROTEIN_TARGETING_TO_MEMBRANE
REACTOME_SIGNALING_BY_INTERLEUKINS
REACTOME_PEPTIDE_LIGAND_BINDING_RECEPTORS
REACTOME_INTERLEUKIN_10_SIGNALING
REACTOME_INTERFERON_GAMMA_SIGNALING
REACTOME_GPCR_LIGAND_BINDING
REACTOME_CYTOKINE_SIGNALING_IN_IMMUNE_SYSTEM
REACTOME_CHEMOKINE_RECEPTORS_BIND_CHEMOKINES
FDR
Log2 fold change
Zanubrutinib vs DMSO
REACTOME_RESPONSE_OF_EIF2AK4_GCN2_TO_AMINO_ACID_DEFICIENCY
REACTOME_PEPTIDE_LIGAND_BINDING_RECEPTORS
REACTOME_NONSENSE_MEDIATED_DECAY_NMD
REACTOME_INTERLEUKIN_4_AND_INTERLEUKIN_13_SIGNALING
REACTOME_INTERLEUKIN_10_SIGNALING
REACTOME_EUKARYOTIC_TRANSLATION_ELONGATION
REACTOME_ELASTIC_FIBRE_FORMATION
REACTOME_CYTOKINE_SIGNALING_IN_IMMUNE_SYSTEM
REACTOME_CHEMOKINE_RECEPTORS_BIND_CHEMOKINES
REACTOME_CELLULAR_RESPONSE_TO_STARVATION
FDR
Log2 fold change

D

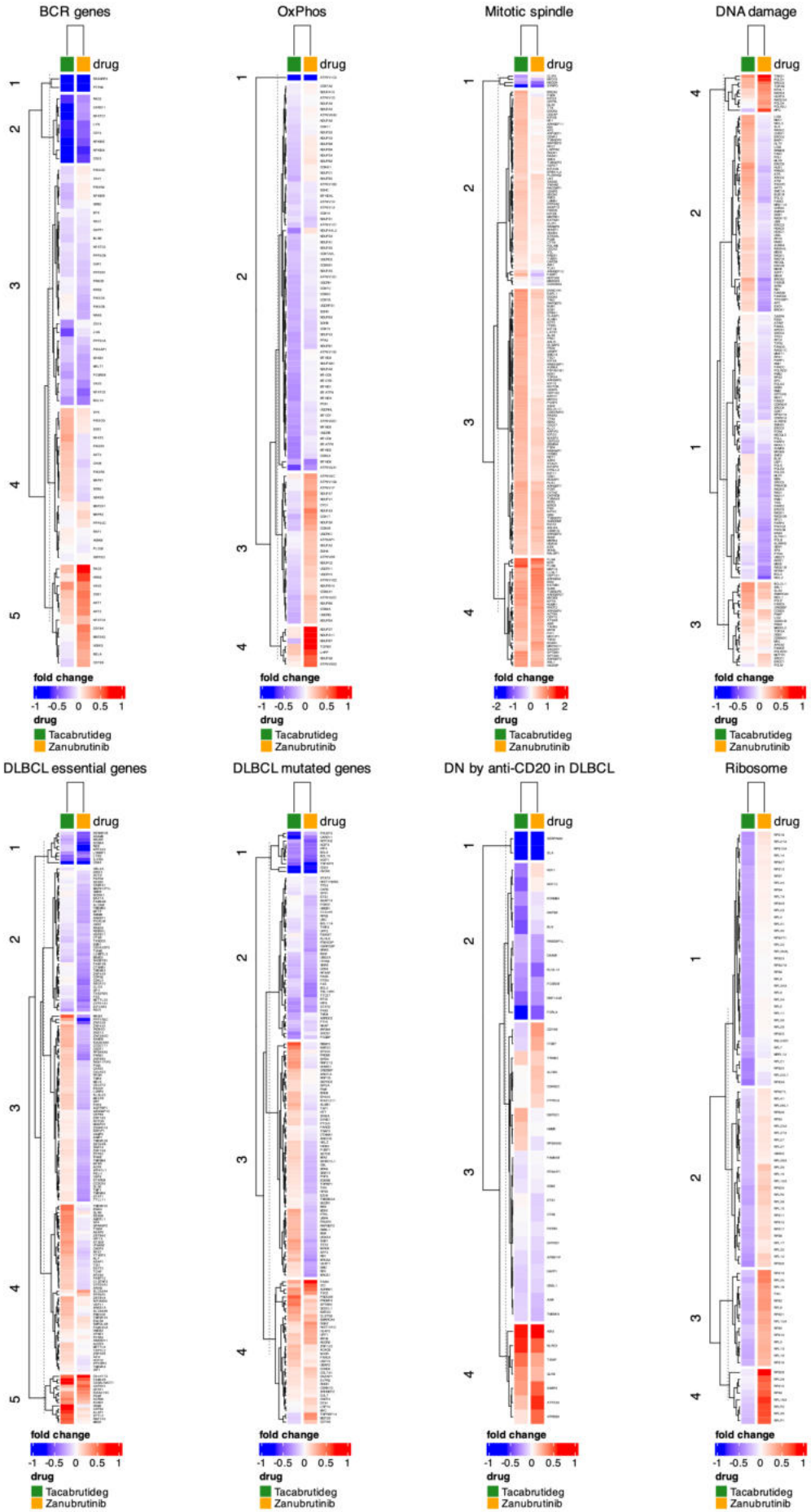
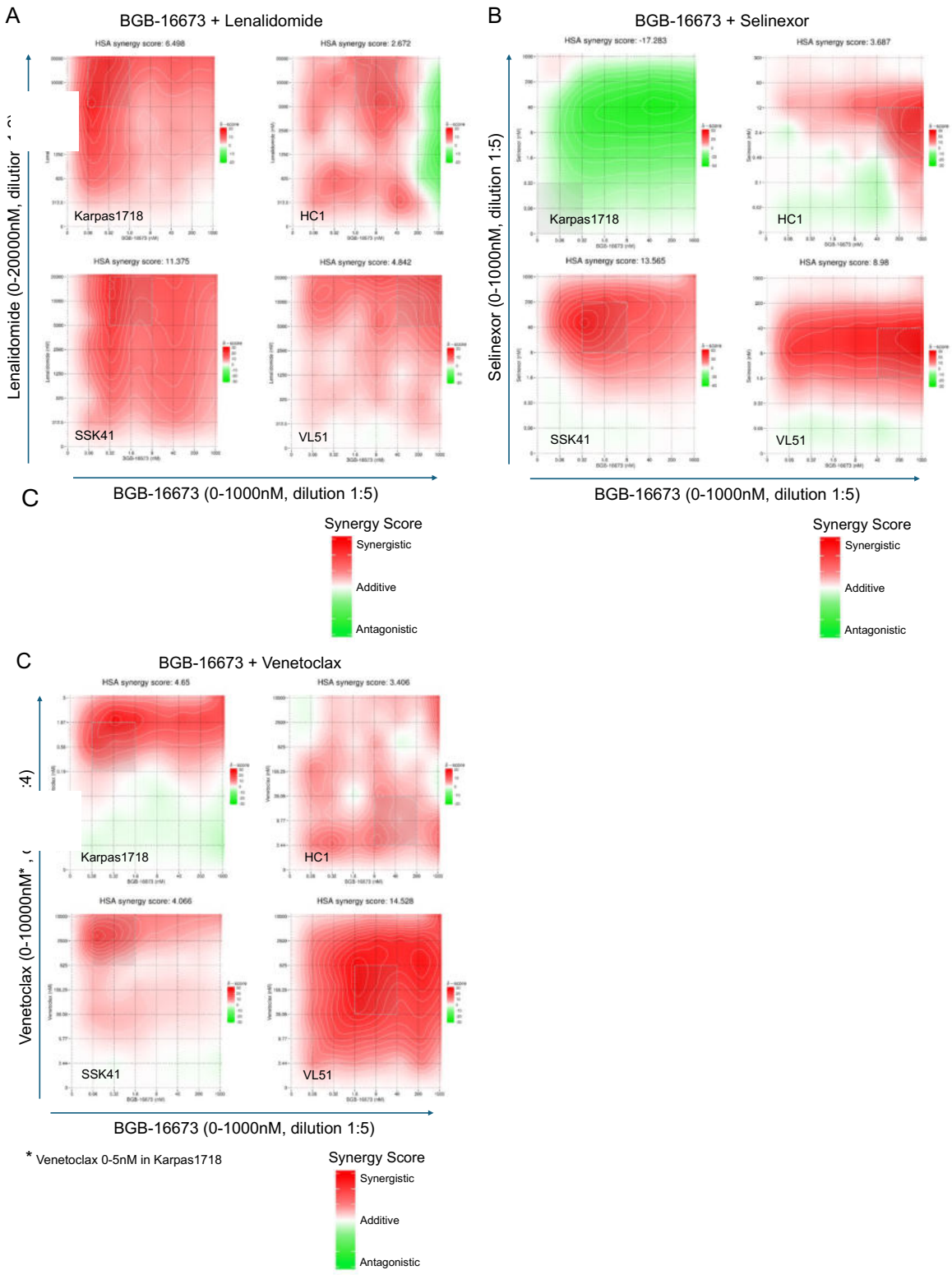
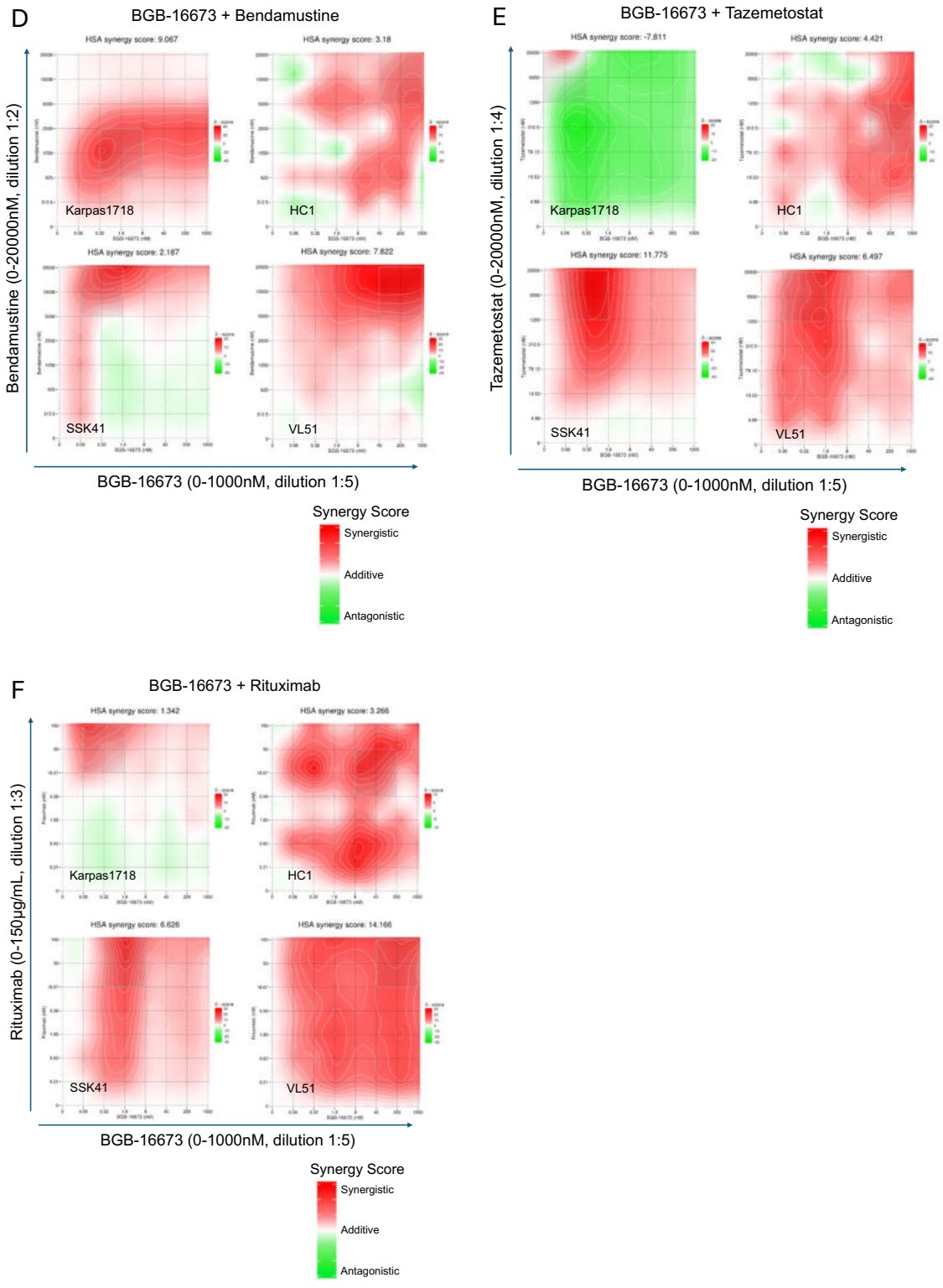
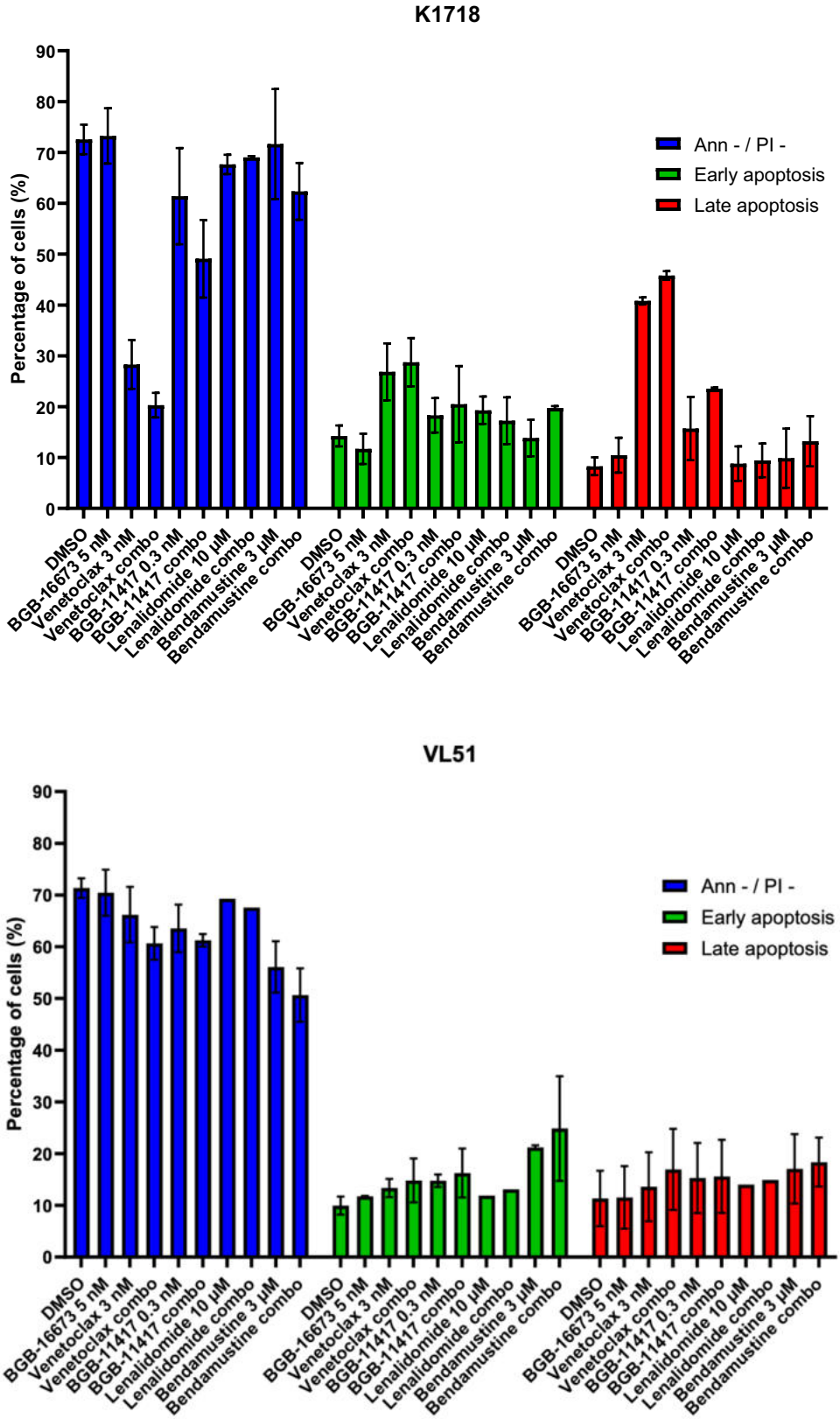

BCR genes
OxPhos
Mitotic spindle
DNA damage
DLBCL essential genes
DLBCL mutated genes
DN by anti-CD20 in DLBCL
Ribosome
drug
fold change
-1 -0.5 0 0.5 1
-2 -1 0 1 2
drug
Tacabrutideg
Zanubrutinib

Figure 6. Effect of the combination of tacabrutideg (BGB-16673) with a series of agents used in clinical settings or clinical development. Karpas1718, HC1, SSK41, and VL51 MZL cell lines were exposed to increasing concentrations of the BTK degrader and a series of clinically relevant agents for five days, followed by an MTT assay. Tacabrutideg was combined with lenalidomide (A), selinexor (B), venetoclax (C), bendamustine (D), tazemetostat (E), and rituximab (F). The benefit of the combination was assessed according to the Highest Single Agent (HSA) algorithm in the Synergy Finder online tool (https://synergyfinder.aittokallio.group/). Red for synergistic, green for antagonistic.

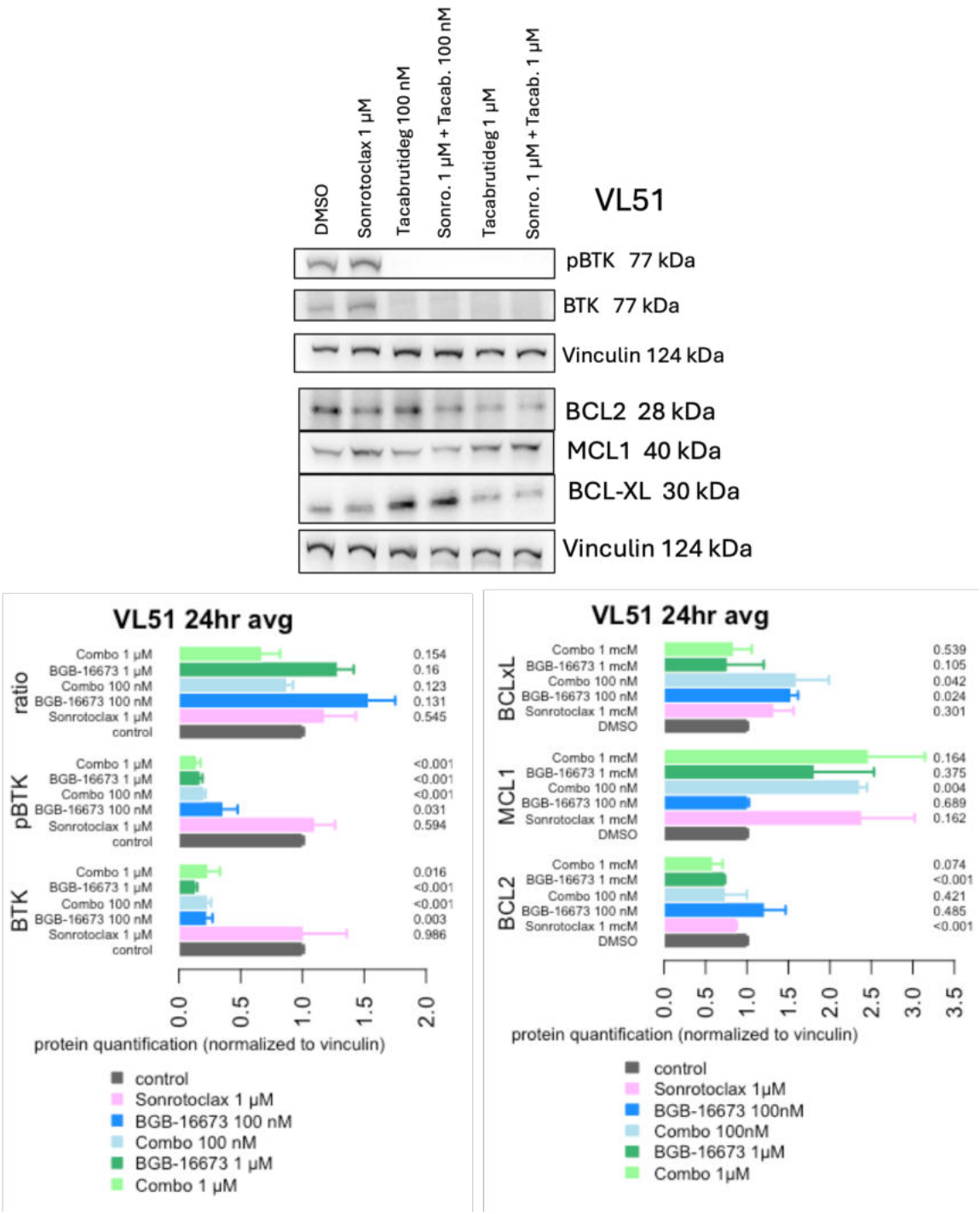



D
BGB-16673 + Bendamustine
HSA synergy score: 9.067
HSA synergy score: 3.18
Karpas1718
HC1
HSA synergy score: 2.187
HSA synergy score: 7.822
SSK41
VL51
Bendamustine (0-20000nM, dilution 1:2)
BGB-16673 (0-1000nM, dilution 1:5)
Synergy Score
Synergistic
Additive
Antagonistic
E
BGB-16673 + Tazemetostat
HSA synergy score: -7.811
HSA synergy score: 4.421
Karpas1718
HC1
HSA synergy score: 11.775
HSA synergy score: 6.497
SSK41
VL51
Tazemetostat (0-20000nM, dilution 1:4)
BGB-16673 (0-1000nM, dilution 1:5)
Synergy Score
Synergistic
Additive
Antagonistic
F
BGB-16673 + Rituximab
HSA synergy score: 1.342
HSA synergy score: 3.266
Karpas1718
HC1
HSA synergy score: 6.626
HSA synergy score: 14.166
SSK41
VL51
Rituximab (0-150µg/mL, dilution 1:3)
BGB-16673 (0-1000nM, dilution 1:5)
Synergy Score
Synergistic
Additive
Antagonistic

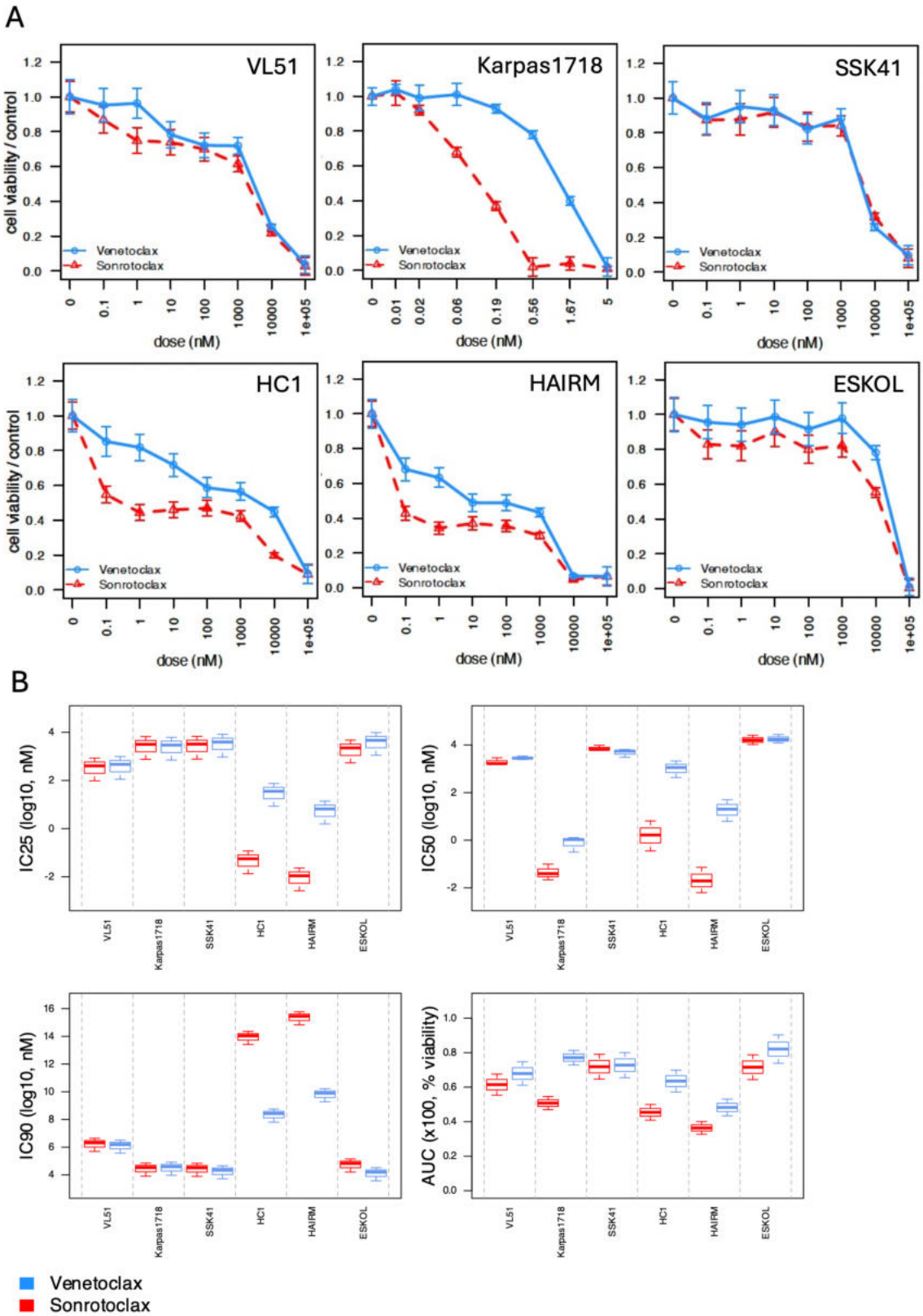
Supplementary Figure 7. Apoptosis induction by tacabrutideg (BGB-16673) as a single agent and in combination with venetoclax, sonrotoclax, or bendamustine in Karpas1718 (upper panel) and in the VL51 (lower panel) cell lines. Barplots show the mean of two biological replicates after 24 hours of treatment. Error bars represent the standard deviation of the mean.



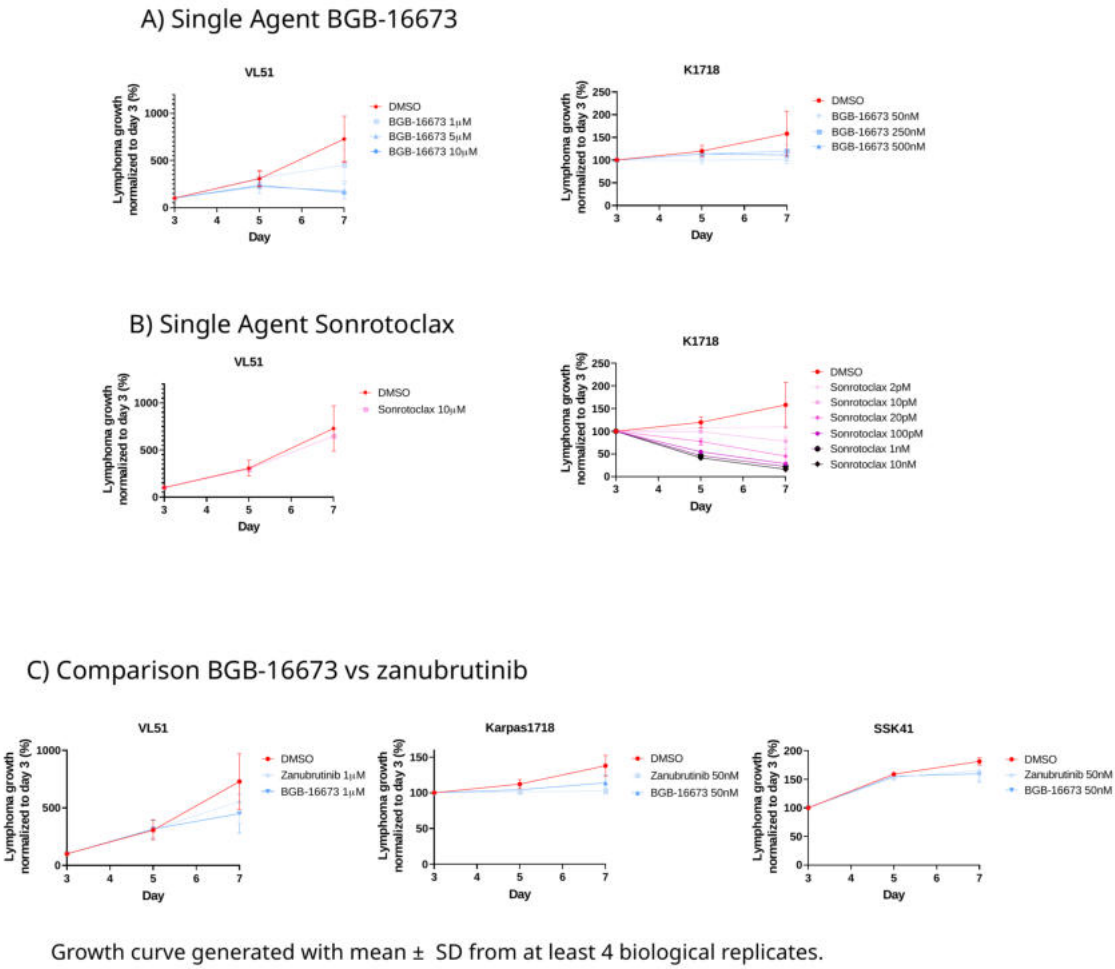
Supplementary Figure 8. Effect of the BTK-degrader tacabrutideg (BGB-16673) and the BCL2 inhibitor Sonrotoclax on the protein levels of BTK/pBTK, BCL2, MCL1, and BCLXL in the MZL cell line VL51 (24hr). Immunoblotting is representative of two independent experiments. The bar plot at the bottom shows the mean protein quantification across the two experiments. Error bars correspond to the standard deviation of the mean. Statistical significance was determined by one-way ANOVA followed by Dunnett's multiple-comparison test, compared to the control (DMSO, grey bar). * P < 0.05; ** P < 0.01; *** P < 0.001; ns, not significant.



Supplementary Figure 9. Effect of five days of exposure to the BCL2 inhibitors sonrotoclax and venetoclax in six MZL cell lines. (A) Drug response curves, (B) Boxplots with sensitivity parameters (AUC for Area under the curve). MTT after 5 days of exposure. Red, sonrotoclax. blue, venetoclax.



Supplementary Figure 10. Single-agent activity of tacabrutideg (BGB-16673, A), sonrotoclax (B) and zanubrutinib (C) in a three-dimensional co-culture system of MZL cell lines with human bone marrow stromal cells. VL51, Karpas1718, and SSK41 cells were cultured with stromal cells and treated with the indicated drugs. Growth curves were generated as mean +/- SD from at least four biological replicates.

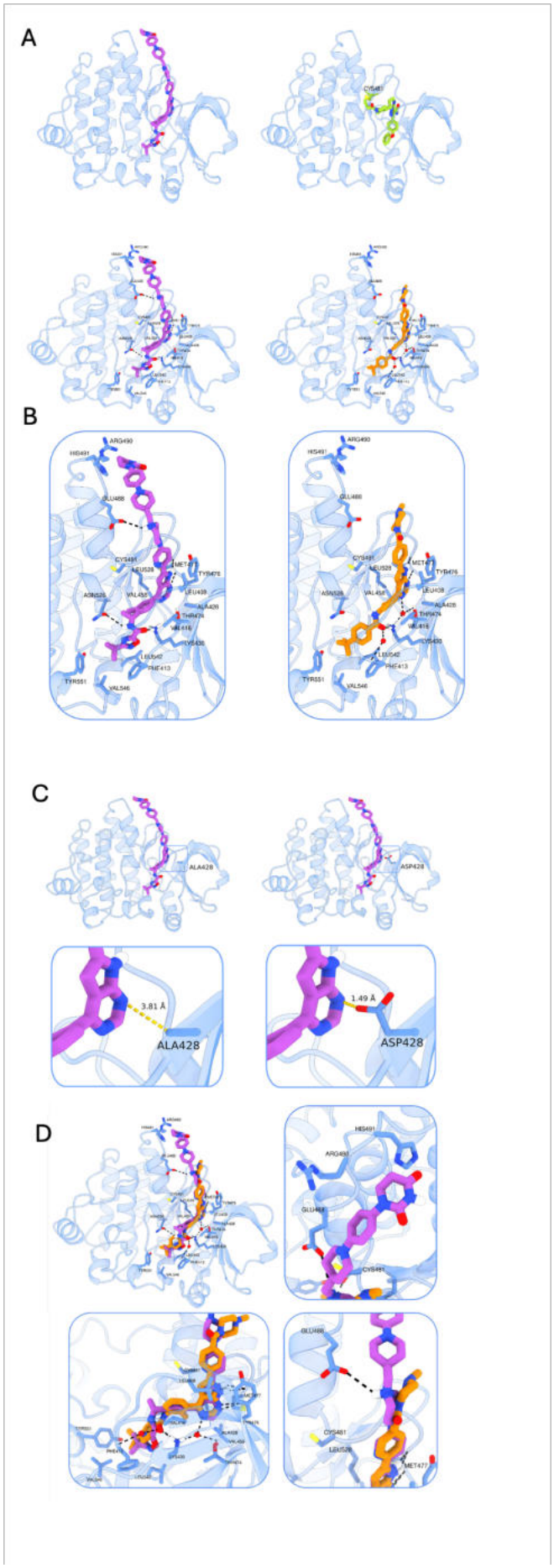


Growth curve generated with mean ± SD from at least 4 biological replicates.

Supplementary Figure 11.

Tacabrutideg binding mode to human BTK. (A) Binding mode of tacabrutideg (purple sticks) to BTK predicted by docking calculations. The crystallographic binding mode of zanubrutinib (PDB ID: 6J6M) (green sticks) to BTK. The BTK protein is shown as light blue ribbons with the Cys481 residue covalently bound to zanubrutinib represented as green sticks. (B) Three-dimensional representation of the binding conformation of tacabrutideg predicted by docking calculations and the crystallographic binding mode of the BTK-inhibitor L0Z (PDB ID: 6S90) within the BTK binding site. The protein is depicted as light blue ribbons, with side chains of interacting residues highlighted as blue sticks; tacabrutideg and L0Z are shown in purple and orange sticks, respectively. Protein–ligand interactions are illustrated as black dashed lines. For clarity, only hydrogen atoms directly involved in interactions are displayed. (C) Representation of the binding mode of tacabrutideg in wild-type BTK and in the *A428D* mutant. The ligand pose in the mutant binding site was obtained by superimposing the wild-type tacabrutideg-BTK complex obtained from docking calculations onto the *A428D* BTK model. The protein is displayed as light blue ribbons, while the side chains of wild-type ALA428 and mutant ASP428 are highlighted as blue sticks; tacabrutideg is shown in purple sticks. Ligand-residue distances are illustrated as yellow dashed lines.

(D) Superimposition of the binding pose of tacabrutideg (BGB-16673) predicted by docking calculations with the crystallographic binding mode of L0Z (PDB ID: 6S90) to BTK. The BTK protein is depicted as light blue ribbons, with key residues highlighted in blue sticks. BGB-16673 and L0Z are represented by purple and orange sticks, respectively. Key receptor–ligand interactions are depicted as black dashed lines. For clarity, only hydrogen atoms directly involved in these interactions are shown. The protein-drug interaction sites are highlighted as insets.


A
B
C
3.81 Å
ALA428
1.49 Å
ASP428
D

Supplementary Table S1. Drug concentrations range and dilutions used in the single treatments and in the combinations with the BTK-degrader tacabrutideg.

experiment	compound	cell line	max concentration	drug dilution
single	Tacabrutideg	all models	10000nM	dil 1/10
single	BGB-21704	Karpas1718, SSK41	10000nM	dil 1/10
single	Zanubrutinib	Karpas1718, SSK41	10000nM	dil 1/10
single	Sonrotoclax	Karpas1718, SSK41, HC1, VL51	10000 (5nM in Karpas1718)	dil 1/4 (dil 1/3 in Karpas1718)
single	Venetoclax	Karpas1718, SSK41, HC1, VL51	10000 (5nM in Karpas1718)	dil 1/4 (dil 1/3 in Karpas1718)
combo with tacabrutideg (0-1000nM dil 1/5)	Lenalidomide	Karpas1718, SSK41, HC1, VL51	20000nM	dil 1/2
combo with tacabrutideg (0-1000nM dil 1/5)	Selinexor	Karpas1718, SSK41, HC1, VL51	1000nM (300nM in HC1)	dil 1/5
combo with tacabrutideg (0-1000nM dil 1/5)	Venetoclax	Karpas1718, SSK41, HC1, VL51	10000 (5nM in Karpas1718)	dil 1/4 (dil 1/3 in Karpas1718)
combo with tacabrutideg (0-1000nM dil 1/5)	Sonrotoclax	Karpas1718, SSK41, HC1, VL51	10000 (5nM in Karpas1718)	dil 1/4 (dil 1/3 in Karpas1718)
combo with tacabrutideg (0-1000nM dil 1/5)	Bendamustine	Karpas1718, SSK41, HC1, VL51	20000nM	dil 1/2
combo with tacabrutideg (0-1000nM dil 1/5)	Tazemetostat	Karpas1718, SSK41, HC1, VL51	20000nM	dil 1/4 (dil 1/3 in Karpas1718)
combo with tacabrutideg (0-1000nM dil 1/5)	Rituximab	Karpas1718, SSK41, HC1, VL51	150µg/mL	dil 1/3

Supplementary Table S2. IC50 values obtained after five days of exposure to the BTK-degrader tacabrutideg or to the BTK inhibitor Zanubrutinib in cell lines derived from MZL (VL51, SSK41, Karpas1718, HC1, HAIRM, ESKOL) and from MCL (REC1, MINO).

compound	sample	IC50 (nM)	se (nM)
Tacabrutideg	Karpas1718	1.8866	0.1505
	SSK41	0.2668	0.1015
	VL51	>1000	-
	ESKOL	>1000	-
	HAIRM	>1000	-
	HC1	>1000	-
	REC1	0.0014	0.0170
	MINO	0.0315	0.0075
Zanubrutinib	Karpas1718	2.5486	2.5486
	SSK41	0.1592	0.1592
	REC1	0.2204	0.2204
	MINO	2.2631	2.2631

Supplementary Table S3 (Excel file). Limma analysis and Gene Set Enrichment Analyses (GSEA) of RNA-Seq data from the MZL cell line Karpas1718 exposed to tacabrutideg (5 nM) or zanubrutinib (5 nM) compared to DMSO. Cells were treated for 8, 12, and 24 hours.

Supplementary Table S4. IC50 values obtained after five days of exposure to the BCL2 inhibitors sonrotoclax and venetoclax in six MZL cell lines.

compound	histology	cell line	IC50 (nM)	se (nM)
Sonrotoclax	MZL	VL51	1646.4	431.9
	MZL	Karpas1718	0.0218	0.0233
	MZL	SSK41	6281.6	1142.2
	MZL	HC1	1.6540	1.8719
	MZL	HAIRM	0.0195	0.0202
	MZL	ESKOL	16015.1	4437.8
Venetoclax	MZL	VL51	2446.3	291.7
	MZL	Karpas1718	1.0663	0.2936
	MZL	SSK41	5494.1	1025.5
	MZL	HC1	1129.7	491.2
	MZL	HAIRM	20.085	13.028
	MZL	ESKOL	17158.4	4536.3